



1 The sensitivity of primary productivity in  
2 Disko Bay, a coastal Arctic ecosystem to  
3 changes in freshwater discharge and sea  
4 ice cover

5

6 Eva Friis Møller<sup>1</sup>, Asbjørn Christensen<sup>2</sup>, Janus Larsen<sup>1</sup>, Kenneth D. Mankoff<sup>3,4</sup>, Mads Hvid  
7 Ribergaard<sup>5</sup>, Mikael Sejr<sup>1</sup>, Philip Wallhead<sup>6</sup>, Marie Maar<sup>1</sup>

8 <sup>1</sup>Department of Ecoscience, Aarhus University, 4000 Roskilde, Denmark

9 <sup>2</sup>DTU Aqua, Technical University of Denmark, DK-2880 Kgs. Lyngby, Denmark

10 <sup>3</sup>Department of Glaciology and Climate, Geological Survey of Denmark and Greenland, 1350  
11 Copenhagen, Denmark

12 <sup>4</sup>National Snow and Ice Data Center (NSIDC), Cooperative Institute for Research in  
13 Environmental Sciences (CIRES), University of Colorado Boulder, Boulder, CO, 80390, USA

14 <sup>5</sup>Danish Meteorological Institute, 2100 Copenhagen, Denmark

15 <sup>6</sup>Section for Oceanography, Norwegian Institute for Water Research (NIVA Vest), Bergen,  
16 Norway

17 *Correspondence to:* Eva Friis Møller ([efm@ecos.au.dk](mailto:efm@ecos.au.dk))



18 **Abstract.** The Greenland Ice Sheet is melting, and the rate of ice loss has increased 6-fold since  
19 the 1980s. At the same time, the Arctic sea ice extent is decreasing. Melt water runoff and sea ice  
20 reduction both influence light and nutrient availability in the coastal ocean with implications for  
21 the timing, distribution and magnitude of phytoplankton production. However, the integrated  
22 effect of both glacial and sea ice melt is highly variable in time and space, making it challenging  
23 to quantify. In this study, we evaluate the relative importance of these processes for the primary  
24 productivity of Disko Bay, West Greenland, one of the most important areas for biodiversity and  
25 fisheries around Greenland. We use a high-resolution 3D coupled hydrodynamic-biogeochemical  
26 model for 2004 to 2018 validated against *in situ* observations and remote sensing products. The  
27 model estimated net primary production (NPP) varied between 90-147 gC m<sup>-2</sup> year<sup>-1</sup> during  
28 2004-2018, a period with variable freshwater discharges and sea ice cover. NPP correlated  
29 negatively with sea ice cover, and positively with freshwater discharge. Fresh water discharge  
30 had a strong local effect within ~25 km of the source sustaining productive hot spot during  
31 summer. When considering the annual NPP at bay scale, sea ice cover was the most important  
32 controlling factor. In scenarios with no sea ice in spring, the model predicted ~30% increase in  
33 annual production compared to a situation with high sea ice cover. Our study indicates that  
34 decreasing ice cover and more freshwater discharge can work synergistically and will likely  
35 increase primary productivity of the coastal ocean around Greenland.



## 36 1 Introduction

37 The warming of the Arctic (Cohen et al., 2020) has a strong impact on the regional sea ice. Over  
38 the past few decades, the sea ice melt season has lengthened (Stroeve et al., 2014), summer  
39 extent has declined, and the ice is getting thinner (Meier et al., 2014). This has an immediate  
40 effect on the primary producers of the ocean. The photosynthetic production is constrained by  
41 the annual radiative cycle, and the sea ice reduces the availability of light and thereby the  
42 development of the sea ice algae and the pelagic phytoplankton communities (Ardyna et al.,  
43 2020). An extended open water period will affect the phenology of primary producers and  
44 potentially lead to an earlier spring bloom (Ji et al., 2013; Leu et al., 2015), and may also  
45 increase the potential for autumn blooms (Ardyna et al., 2014).

46 In the Arctic coastal ocean, there are additional impacts of a warming climate. As the freshwater  
47 discharge increases due the melt of snow and ice on land and higher precipitation (Kjeldsen et  
48 al., 2015; Mankoff et al., 2020a, 2021), the land-ocean coupling along the extensive Arctic  
49 coastline is intensified (Hernes et al., 2021). The summer inflow of melt water has complex  
50 biogeochemical impacts on the coastal ecosystem and combines with changes in sea ice cover to  
51 affect the magnitude and phenology of marine primary production. In areas dominated by  
52 glaciated catchments such as Greenland, the increase in melt water discharge has been  
53 substantial and the rate of ice mass loss has increased sixfold since the 1980s (Mankoff et al.,  
54 2020b; Mouginit et al., 2019).

55 The changes in sea ice cover and freshwater discharge will affect the marine primary production  
56 through the complex interactions of changes in stratification, light and nutrient availability  
57 (Arrigo and van Dijken, 2015; Hopwood et al., 2020). The individual processes are relatively  
58 well described, but the interactions between them and the temporal and spatial importance under  
59 different Arctic physical regimes are less well understood. A lower extent of sea ice cover may  
60 also increase the wind induced mixing of the water column and deepen or weaken the  
61 stratification. Thereby, the potential for the phytoplankton to stay and grow in the illuminated  
62 surface layer is reduced. At the same time, a higher mixing rate will increase the supply of new  
63 nutrients from deeper layers to support production when light is not limiting (Tremblay and  
64 Gagnon, 2009). Another mechanism affecting stratification is the freshening of the surface layer  
65 due to ice melt from both sea ice and the ice sheet (von Appen et al., 2021; Holding et al., 2019).



66 However, if a glacier terminates in a deep fjord, the ice sheet melt is injected at depth causing  
67 more coastal upwelling of nutrients before acting to increase surface layer stratification  
68 (Hopwood et al., 2018; Meire et al., 2017)

69 The relative importance on productivity of sea ice versus glacier freshwater discharge depends  
70 on the scale considered (Hopwood et al., 2019). Freshwater discharge from the ice sheet is more  
71 important in the vicinity of the glacier (Hopwood et al., 2019; Meire et al., 2017), whereas the  
72 sea ice dynamics are considered to be an important driver in the open ocean (Arrigo and van  
73 Dijken, 2015; Massicotte et al., 2019; Meier et al., 2014). Most studies consider one or the other  
74 separately (e.g. Hopwood et al., 2018; Vernet et al., 2021). However, in the coastal Arctic areas  
75 at the mesoscale, i.e. 10-100 km, it can be expected that both sea ice and glacier freshwater  
76 discharge and the interaction between them will influence the ecosystem and the pelagic primary  
77 production (Hopwood et al., 2019). To resolve their relative impacts, we need to constrain their  
78 impact on both seasonal and spatial scales, which is a challenging task. A useful tool to achieve  
79 such an integrated perspective is a high-resolution 3D coupled hydrodynamic-biogeochemical  
80 model.

81 Disko Bay is located on the west coast of Greenland (Fig. 1) near the southern border of the  
82 maximum annual Arctic sea ice extent, and is influenced by both sub-Arctic waters from  
83 southwestern Greenland and Arctic waters within the Baffin Bay (Gladish et al., 2015; Rysgaard  
84 et al., 2020). The bay has a pronounced seasonality in sea ice cover (Møller and Nielsen, 2020).  
85 Over the last 40 years, there has been pronounced decrease in sea ice cover, and also the year-to-  
86 year variations have increased in the last decade (Fig 2, Hansen et al., 2006, the Greenland  
87 Ecosystem monitoring program, <http://data.g-e-m.dk>). For the primary producers particularly the  
88 decrease in sea ice cover during the time of the spring bloom in April is important (Møller and  
89 Nielsen, 2020). In addition to the seasonal sea ice cover changes, the bay also experiences large  
90 seasonal changes in freshwater input from the Greenland ice sheet, particularly during the  
91 summer months (Fig. 2, 3). The large marine terminating glacier Sermeq Kujalleq (Jakobshavn  
92 Isbræ) is found in the inner part of the bay. It is estimated that about 10% of the icebergs from  
93 the Greenland ice sheet originate from this glacier (Mankoff et al., 2020a). Since the 1980s,  
94 freshwater discharge from the Greenland Ice sheet to Disko Bay has almost doubled (Fig. 2,  
95 (Mankoff et al., 2020b, 2020a). How these significant changes in sea ice dynamics and run-off



96 will impact the ecosystem in Disko Bay, one of the most important areas for biodiversity and  
97 fisheries around Greenland (Christensen et al. 2012), is still not well understood.

98 In this study, we investigate the combined effect of changes in sea ice cover and the Greenland  
99 ice sheet freshwater discharge on the phenology/seasonal timing and annual magnitude and  
100 spatial distribution of the phytoplankton production in Disko Bay. We do so using a high-  
101 resolution 3D coupled hydrodynamic-biogeochemical model validated against in situ  
102 measurement of salinity, temperature, nutrients, phytoplankton, and zooplankton biomass. The  
103 validated model allows us to estimate the impact of sea ice cover and freshwater discharge on  
104 productivity with a higher temporal and spatial resolution than would be possible from  
105 measurements alone.

## 106 2 Methods

### 107 2.1 Hydrodynamic model

108 The model was set up using the FlexSem model system (Larsen et al. 2020). FlexSem is an open  
109 source modular framework for 3D unstructured marine modelling  
110 (<https://marweb.bios.au.dk/flexsem>). The system contains modules for hydrostatic and non-  
111 hydrostatic hydrodynamics, 3D pelagic and 3D benthic models, sediment transport and agent-  
112 based models. The source code can be found at the FlexSem webpage.

113 Bathymetry were obtained from the 150x150 m resolved IceBridge BedMachine Greenland,  
114 Version 3 (<https://nsidc.org/data/IDBMG4> (Morlighem et al., 2017)) and interpolated to the  
115 FlexSem computational mesh using linear interpolation. The 96,300 km<sup>2</sup> large computational  
116 mesh for the Disko Bay area was constructed using the mesh generator JigSaw  
117 (<https://github.com/dengwirda/jigsaw>) (Fig. 1). It consists of 6349 elements and 34 depth z-  
118 layers with a total of 105678 computational cells. The horizontal resolution varies from 1.8 km  
119 in the Disko Bay proper, 4.7 km in Strait of Vaigat and 16 km towards the semi-circular Baffin  
120 Bay open boundary. In the deepest layers, the vertical resolution is 50 m, decreasing towards the  
121 surface, where the top 5 layers are 3.5, 1.5, 2.0, 2.0 and 2.0 meters thick, respectively. The  
122 surface layer thickness is flexible allowing changes in water level e.g., due to tidal elevations.  
123 The model time step is 300 seconds and has been run for the period from 2004 to 2018.



## 124 **2.2 Biogeochemical model**

125 The biogeochemical model in the FlexSem framework was based on a modification of the  
126 ERGOM model that originally was applied to the Baltic Sea and the North Sea (Maar et al.,  
127 2011, 2016; Neumann, 2000) (Appendix A). In the Disko Bay version, 11 state variables  
128 describe concentrations of four dissolved nutrients ( $\text{NO}_3$ ,  $\text{NH}_4$ ,  $\text{PO}_4$ ,  $\text{SiO}_2$ ), two functional groups  
129 of phytoplankton (diatoms, flagellates), micro- and mesozooplankton, detritus (NP), detritus-  
130 silicon, and oxygen. Cyanobacteria present in the Baltic Sea version of the model are removed in  
131 the current set-up, because cyanobacteria are of little importance in high-saline Arctic waters  
132 (Lovejoy et al., 2007). Further, pelagic detrital silicon was added to better describe the cycling  
133 and settling of Si in deep waters. The model currency is N using Redfield ratios to convert to P  
134 and Si. Chlorophyll *a* (Chl *a*) was estimated as the sum of the two phytoplankton groups  
135 multiplied by a factor of 1.7 mg-Chl/mmol-N (Thomas et al., 1992). The calanoid copepod *C.*  
136 *finmarchicus* generally dominates the mesozooplankton biomass (Møller and Nielsen, 2020) and  
137 the physiological processes were parameterized according to previous studies (Møller et al.,  
138 2012, 2016). The model considers the processes of nutrient uptake, growth, grazing, egestion,  
139 respiration, recycling, mortality, particle sinking and seasonal mesozooplankton migration in the  
140 water column and overwintering in bottom waters. NPP was estimated as daily means of  
141 phytoplankton growth after subtracting respiration and integrated over 30 m depth corresponding  
142 to the productive layer. The timing of the seasonal *C. finmarchicus* migration was calibrated  
143 against in situ measurements of their vertical distribution over time (Møller and Nielsen, 2019).  
144 Light attenuation ( $k_d$ ) is a function of background attenuation (water turbidity,  $k_{db}$ ) and  
145 concentrations of detritus and Chl *a* (Maar et al., 2011). Turbidity is strongly correlated with  
146 salinity and the background attenuation was described as a function of salinity:  $k_{db}=0.80\text{-salinity}$   
147  $\times 0.0288$  for salinity  $< 25$  and a constant of  $0.08 \text{ m}^{-1}$  for salinity  $>25$  according to monitoring  
148 data in the Disko Bay  $69^\circ 14' \text{ N}$ ,  $53^\circ 23' \text{ W}$  (data.g-e-m.dk) and measurements across a salinity  
149 gradient in another Greenland fjord, the Young Sound (Murray et al., 2015). Light optimum was  
150 changed for both phytoplankton groups during calibration to fit with the timing of the spring  
151 bloom (Appendix A). Background mortality of microzooplankton was increased to account for  
152 other grazing pressure than from *C. finmarchicus*.



### 153 **2.3 Freshwater and nutrient discharge**

154 We used the MAR and RACMO regional climate model (RCM) runoff field to compute  
155 freshwater discharge. Ice runoff is defined as ice melt + condensation – evaporation + liquid  
156 precipitation – refreezing. Land runoff is computed similarly, but there is no ice melt term  
157 (although there is snow melt). Daily simulations of runoff were routed at stream scale to coastal  
158 outlets, where it is then called ‘discharge’. Precipitation onto the ocean surface is not included in  
159 the calculations (Mankoff et al., 2020a) Within Disko Bay, 235 streams discharge liquid water,  
160 of which 97.5 % of the water comes from just 30 streams.

161 Fourteen points were selected within the model domain to represent the freshwater inflow. The  
162 locations were manually selected to best represent the location of the largest rivers and the  
163 spatial distribution of freshwater inflow in the model domain. The inflow from the 30 largest  
164 rivers were manually aggregated into the 14 point sources by evaluating the geographical  
165 location in relation to the coastal layout. This land run-off was inserted into the nearest model  
166 cell in the surface layer. Although subglacial discharge enters at depth, it rises up the ice front  
167 within a few 10s to 100s of meters of the ice front and within the grid cell at the ice boundary  
168 will reach its neutral isopycnal here assumed to be the surface layer (Mankoff et al., 2016). Thus,  
169 ice runoff were inserted in the surface layer. Solid ice discharge was computed from ice velocity,  
170 ice thickness, and ice density at marine terminating glaciers (Mankoff et al., 2020b). Within our  
171 modelling area in Disko Bay four glaciers discharge icebergs into fjords, of which the majority  
172 comes from Sermeq Kujalleq (Jakobshavn Isbræ). Solid ice was inserted where glaciers  
173 terminate directly into fjords (Fig. 1). At these four localities with marine terminating, the  
174 freshwater contribution as solid ice was assumed to be equally distributed in the top 100 m  
175 assuming that the majority of the solid ice are small pieces that melts quickly as evidenced by the  
176 lack of brash ice generally seen in Disko Bay. Thus, we do not consider the large icebergs calved  
177 by Sermeq Kujalleq and their input of freshwater along the route in the bay. Land discharge of  
178 nitrate, phosphate, and silicate at the 14 point sources was assumed to be constant in time with  
179 concentrations of 1.25, 0.20 and 10.88 mmol m<sup>-3</sup>, respectively (Hopwood et al., 2020).

### 180 **2.4 Hydrodynamic open boundary and initial data**

181 At the semi-circular open boundary towards the Baffin Bay, the model was forced with ocean  
182 velocities, water level, salinity, and temperature obtained from a coupled ocean- and sea-ice



183 model (Madsen et al., 2016) provided by the Danish Meteorological Institute (DMI). The DMI  
184 model system consists of the HYbrid Coordinate Ocean Model (HYCOM, e.g., Chassignet et al.,  
185 2007) and the Community Ice CodE (CICE, (Hunke, 2001; Hunke and Dukowicz, 1997) coupled  
186 with the Earth System modeling Framework (ESMF) coupler (Collins et al., 2005). The  
187 HYCOM-CICE set-up at DMI covers the Arctic Ocean and the Atlantic Ocean, north of about  
188 20°S, with a horizontal resolution of about 10 km. Further details on the HYCOM-CICE model  
189 system can be found in Appendix B.

190 The 2D (water level) and 3D parameters were interpolated to match the open boundary in the  
191 FlexSem Model setup using linear interpolation. Correspondingly, initial fields of temperature,  
192 salinity and water level were interpolated from the HYCOM-CICE model output.

## 193 **2.5 Observed sea ice cover**

194 The long term sea ice cover within Disko Bay was extracted from the sea-ice concentration data  
195 provided by the EUMETSAT Ocean and Sea Ice Satellite Application Facility (OSISAF,  
196 www.osi-saf.org, Lavergne et al., 2019) on a daily basis (AICE). The Disko Bay area is here  
197 defined as longitude and latitude range between 54.0°W and 51.5°W and 68.7°N to 69.5°N  
198 respectively. As the OSISAF product is seasonally quite noisy for low sea ice concentrations, we  
199 made a cutoff at 40 percent before we take the mean for the entire area. The exact cut-off value  
200 does not matter much on the resulting time series, as the freeze-up and melt-down period is quite  
201 fast for the area. Furthermore, we obtained sea ice observations from the Greenland Ecosystem  
202 Monitoring (GEM) program (<http://data.g-e-m.dk>) in which ice coverage is registered daily by  
203 visual inspection from the laboratory building at Copenhagen University's Arctic station in  
204 Qeqertarsuaq.

## 205 **2.6 Surface forcing data**

206 At the surface, the model was forced by sea ice concentration, wind drag and heat fluxes. The ice  
207 cover percentage modifies the wind drag, heat balance and light penetration in the model. The  
208 surface heat budget model estimating the heat flux (long- and short-wave radiation) was forced  
209 by wind, 2 meter atmospheric temperature, cloud cover, specific humidity and ice cover.  
210 Photosynthetically active radiation (PAR) was estimated from the short-wave radiation assuming  
211 43% to be available for photosynthesis (Zhang et al., 2010). The atmospheric forcing was  
212 provided by DMI from the HIRLAM (Yang et al., 2005) and HARMONIE (Yang et al., 2017;





213 2018) meteorological models using the configuration with the best resolution available for our  
214 simulation period. The resolution was 15 km until May 2005, then increased to about 5 km until  
215 March 2017, and since then to 2.5 km. Ice cover was obtained from the HYCOM-CICE model  
216 output.

## 217 **2.7 Biogeochemical open boundary and initial data**

218 Initial data and open boundary conditions for ecological variables were obtained from the pan-  
219 Arctic ‘A20’ model at NIVA Norway. This was based on a 20 km-resolution ROMS ocean-sea-  
220 ice model (Shchepetkin and McWilliams, 2005, Roed et al., 2014) coupled to the ERSEM  
221 biogeochemical model (Butenschön et al., 2016), run in hindcast mode and bias-corrected  
222 towards a compilation of in situ observations (Palmer et al., 2019). This model provided bias-  
223 corrected output for (nitrate, phosphate, silicate, dissolved oxygen) plus raw hindcast output for  
224 ammonium, detritus (small, medium and large fractions), 6 groups of phytoplankton and 3  
225 zooplankton groups. The picophytoplankton, *Synechococcus*, nano-, micro-phytoplankton and  
226 prymnesiophyte biomasses from ERSEM were summed to provide data for the autotrophic  
227 flagellate group in ERGOM, while the diatom functional group was the same in both models.  
228 The detritus pool in ERGOM was the sum of the three detritus size fractions in ERSEM. The  
229 A20 data were provided as weekly means on a 20 km grid and linearly interpolated to the  
230 FlexSem grid. ERSEM provided data through 2014, then 2014 was repeated for the following  
231 years.

## 232 **2.8 Validation**

233 For model calibration and validation of the seasonality, we used reported research observations  
234 of temperature, salinity, nutrients (nitrate, silicate, phosphate), Chl *a* concentrations and  
235 mesozooplankton biomass collected during short-term field campaigns at the Disko Bay station  
236 69° 14’ N, 53° 23’ W from 2004 to 2012 (e.g.(Møller and Nielsen, 2019)). Furthermore, we used  
237 observations of the same variables from the same station provided by the Greenland Ecological  
238 Monitoring (GEM) program running since 2016 in the Disko Bay (data.g-e-m.dk). However, the  
239 data coverage is highly sporadic between years and months, and we therefore created a monthly  
240 climatology (2004-2018) for the best-sampled depth layer 0-20 m. This climatology was  
241 compared with monthly means extracted from the model at the same location and depth range  
242 where 2004 was used for model calibration and means from 2005 to 2018 for model validation.



243 Mesozooplankton biomass in the model was assumed to mainly represent the copepods *Calanus*  
244 spp. and for the conversion from N to carbon (C) biomass, we used 12 g-C mol<sup>-1</sup> and C:N= 6.0  
245 mol-C mol-N<sup>-1</sup> (Swailethorp et al., 2011).

246 Additionally, the model was validated spatially using remote sensing (RS) data of sea surface  
247 temperature (SST) and Chl *a* concentrations for spring (April to June) and summer (July to  
248 September) for 2010 and 2017. RS data was obtained from the Copernicus Marine Service (ref  
249 <https://marine.copernicus.eu>). For SST we used the L4 product  
250 ‘SEAICE\_ARC\_PHY\_CLIMATE\_L4\_MY\_011\_016-TDS’, which has spatial resolution of 0.05  
251 degree and daily time resolution. For Chl *a* we used the data service  
252 ‘OCEANCOLOUR\_ARC\_CHL\_L4\_REP\_OBSERVATIONS\_009\_088-TDS’ (L4 product  
253 based on the OC5CCI algorithm), which has a spatial resolution of 0.01 degree and monthly time  
254 resolution. Chl *a* concentrations were log-transformed because they span several orders of  
255 magnitude. For both SST and Chl *a* comparisons, the RS data were interpolated to cell center  
256 points of the horizontal FlexSem grid using a bi-linear scheme. Validation was only performed at  
257 spatial points, where RS data has at least one quality-accepted data entry (i.e. sufficient visibility  
258 without ice and cloud cover) for the respective validation periods.

259 The model skill was assessed by different metrics. The Pearson correlation between observations  
260 and model results was estimated for the seasonal data and spatial data assuming a significance  
261 threshold of  $p < 0.05$ . The other metrics were:

262 Mean Error (ME) is the mean of the differences between observations  $x$  and model results  $y$ :

$$263 \quad ME = \frac{1}{N} \sum_{i=1}^N (y_i - x_i)$$

264 where  $N$  is the total number of data points. The Root Mean Square Error (RMSE) is the square  
265 root of the mean squared error between  $x$  and  $y$ :

$$266 \quad RMSE = \sqrt{\frac{1}{N} \sum_{i=1}^N (y_i - x_i)^2}$$

267 The average cost function ( $cf$ ) is defined as (Radach and Moll 2006):



268

$$cf = \frac{1}{N} \sum_{i=1}^N \frac{|(y_i - x_i)|}{SD(x)}$$

269 Depending on the *cf* number, it is possible to assess the performance of the model as “very good”  
270 (<1), “good” (1-2), “reasonable” (2-3), and “poor” (>3).

271 Microzooplankton data was available from the literature for 1996/97 (Levinsen and Nielsen,  
272 2002) and April-May 2011 (Menden-Deuer et al., 2018). Thus, it was not possible to create a  
273 climatology, but the available data was used for visual comparison with model data. Data from  
274 Levinsen and Nielsen (2002) was depth integrated (g-C m<sup>-2</sup>), and converted to mg-C m<sup>-3</sup> by  
275 assuming that the total biomass was distributed uniformly over the upper 25 m (Levinsen et al.,  
276 2000). Data from Menden-Deuer (2018) was from fluorescence maximum, and this was assumed  
277 to represent the upper 20 m. The conversion from nitrogen to carbon biomass was obtained from  
278 the Redfield ratio=6.625 mol-C mol-N<sup>-1</sup> and the mol weight of 12 g-C mol<sup>-1</sup>.

## 279 **2.9 The impact of sea ice cover and discharge on primary productivity**

280 An overall indication of the relationship between NPP and sea ice cover and freshwater  
281 discharge was obtained by Pearson product moment correlation analysis between annual  
282 estimates of these for the entire Bay, as defined by the box in figure 1. We further evaluated the  
283 impact of sea ice cover and freshwater discharge on the NPP on a spatial scale. To do this we  
284 perform correlation analysis between the annual NPP and the average sea ice cover March-April  
285 in each model grid cell for 2004-2018. To evaluate the impact of the discharge we performed  
286 similar correlations with average annual surface salinity instead of sea ice cover. The  
287 assumption behind the choice is that the surface salinity scales with the impact of freshwater  
288 discharge.

289 To demonstrate the effect of sea ice cover and distance to the glacial outlet on the temporal  
290 development of nitrogen concentration, Chl *a*, and NPP, two stations and two years with  
291 different features were selected. The first station was located in the open bay and the other  
292 station close to the Ilulissat Isfjord (Bay and Glacier station, Fig. 1). The two years 2010 and  
293 2017 were chosen according to differences in both irradiance and sea ice cover, one (2010) with  
294 low sea ice cover and high irradiance and the other (2017) with high sea ice cover and low  
295 irradiance.



296 To further evaluate the impact of sea ice cover and freshwater discharge we performed some  
297 simple “extreme” model scenarios (Table 1). We tested the potential effect on primary  
298 productivity in 2010 (low sea ice cover) and 2017 (high sea ice cover) in scenarios with no sea  
299 ice, no freshwater discharge or 2 times the reference discharge, as well as the combinations, by  
300 changing the model forcing accordingly.

### 301 3 Results

#### 302 3.1 Fresh water discharge and sea ice cover

303 50 years ago, the average annual liquid runoff from the ice sheet to the study area was generally  
304  $\sim 1000 \text{ m}^3 \text{ s}^{-1}$  ( $913 \pm 2214 \text{ SD m}^3 \text{ s}^{-1}$ , 1958-1969), whereas during the last 20 years is has varied  
305 between 2000 and  $4500 \text{ m}^3 \text{ s}^{-1}$  ( $2591 \pm 724 \text{ SD m}^3 \text{ s}^{-1}$ , 2000-2019) (Fig. 2). The precipitation over  
306 land has also increased from about 200 ( $197 \pm 40 \text{ SD m}^3 \text{ s}^{-1}$ ) to 400-500  $\text{m}^3 \text{ s}^{-1}$  ( $469 \pm 77 \text{ SD m}^3 \text{ s}^{-1}$ )  
307 <sup>1</sup>). The calving of solid ice from the glaciers has only been estimated for the last 30 years, but it  
308 also shows an increasing trend although since the maximum in 2013, the production of ice has  
309 been lower (Fig. 2). Thus, for all three sources of freshwater the overall long-term trend is an  
310 increase, but for the model period between 2004 and 2018 no trend was evident (Fig. 3e). The  
311 freshwater discharge from solid ice was relatively constant across the year, whereas the liquid  
312 contribution peaked during summer, from June to August, and drops to almost zero in the winter  
313 (Fig. 3f).

314 The sea ice cover in Disko Bay has generally decreased during the last 35 years (Fig. 2).  
315 However, the last 15 years have been characterized by large interannual variation with some  
316 years with virtually no ice and others with sea ice cover as in the 1990s. During the model period  
317 the ice generally did not form before late December, and the maximum ice cover was seen in  
318 March (Fig. 3)

#### 319 3.2 Validation of the model

320 The seasonal timing and general level of temperature, salinity, nutrients, Chl *a* and  
321 mesozooplankton agreed well with the data climatology from the field sampling south of Disko  
322 Island (Fig. 4, Table 2). All correlations between observational and model data were significant  
323 ( $R > 0.82$ ). The model performance assessed by the average cost function *cf* was “very good” for  
324 all parameters. Modelled Chl *a* showed highest interannual variability in spring and the



325 chlorophyll bloom was somewhat too weak (~30% less), and the winter silicate too high, relative  
326 to the climatological mean observations.

327 The spatial distribution patterns of Chl *a* and temperature at the surface were compared to  
328 satellite estimates for the two years 2010 and 2017 used in the scenarios representing low and  
329 high sea ice cover, respectively (Table 3, Fig. C1). The correlations were significant for all  
330 relations ( $p < 0.01$ ), and the *cf* number was “very good” or “good” for all (Table 3). Surface  
331 temperature tended to be higher in spring and lower in summer in the model compared to the  
332 satellite estimates. Chl *a* concentrations were generally higher in the model than in the satellite  
333 data, especially in spring 2017 (Fig. C1).

### 334 **3.3 Seasonal and spatial patterns of NPP in Disko Bay**

335 Primary production starts as sea ice cover decreases and irradiance increases in February (Fig. 3).  
336 Extensive sea cover may reduce light availability in the water column and thereby limit  
337 production, and the interannual variation in NPP is highest in April because of the variation in  
338 sea ice cover, causing light availability in the water to vary accordingly. Highest NPP was in  
339 May and June with about 800 mg-C m<sup>-3</sup> d<sup>-1</sup> when light influx was highest and sea ice was  
340 entirely melted (Fig. 3).

341 The impact of sea ice is illustrated by comparing a year with low (2010) and high (2017) sea ice  
342 cover, where the spring bloom is about 25-30 days earlier in 2010 than in 2017 (Fig. 5).  
343 Comparing a station close to and far from the glacier illustrates the potential impact of the fresh  
344 water peak in late summer, as NPP is 2-3 times higher during this period at the station close to  
345 the glacier (Fig. 5).

346 Concerning the spatial distribution in the spring period (March to June), high NPP was seen  
347 across the bay, with the lowest values found southeast of the Disko Island and southwest of the  
348 Bay following the bathymetry. In the later summer period (July to October), primary production  
349 was more confined to the coast (Fig. 6).

### 350 **3.4 Annual variability of NPP**

351 The annual average NPP in the Bay estimated from the model varied between 90 and 147 g-C  
352 m<sup>-2</sup> year<sup>-1</sup> with an average of 129±16 (SD) (Fig. 3). Generally, years with high sea ice cover in  
353 spring had lower average annual NPP (Fig. 3, Pearson product moment correlation coefficient *r*



354 = -0.63,  $p=0.01$ ), while higher discharge was associated with higher annual primary productivity  
355 (Fig. 3,  $r = 0.51$ ,  $p=0.05$ ).

356 To evaluate the spatial dependency, we performed an analysis of the correlation between the sea  
357 ice cover in March to April and the annual NPP in each model grid cell. This showed a negative  
358 relationship widespread in the model domain, i.e. the more sea ice, the lower NPP (Fig. 7). One  
359 exception was in the south part of the model domain, where the correlation was positive. The  
360 impact of the freshwater discharge on the NPP was generally positive in areas up to ~50 km from  
361 the discharge and additionally in the northern part of Disko Bay, as reflected by the negative  
362 correlation to surface salinity in these areas (Fig. 7).

### 363 **3.5 Model scenarios with sea ice cover and discharge**

364 We studied some simple model scenarios where sea ice cover was assumed to be zero and the  
365 discharge was either doubled or cut off, with basis in 2010 and 2017, which had low and high sea  
366 ice cover, respectively, and opposite discharge (Fig. 3). These scenarios underline the  
367 complexity of the dynamics of the system, with some areas experiencing increased NPP while  
368 others experience a decrease (Figs. 8, 9). Furthermore, it allows us to evaluate the impact of the  
369 uncertainty of actual freshwater runoff. The year 2017 had relatively high and late ice cover (Fig.  
370 3) and applying a scenario of no ice leads to an increase in bay-scale annual NPP of 34 %,  
371 although spatial variability is high and annual NPP changes vary between -20% and 98% (Fig.  
372 9). For 2010, a year that already had low sea ice cover, the same scenario led to minor changes in  
373 the annual NPP on bay scale (2 %, Fig. 8). For both years, the omission of freshwater discharge  
374 generally led to a decrease in annual NPP; this effect was small on the bay scale (-2 to 0%), but  
375 reached -64% in near-coastal areas under glacial/runoff influence. Similarly, the effect of  
376 doubling of the discharge was minor on the bay scale (0-1%), but reached up to 55 and 68 %  
377 NPP increase in runoff-influenced areas in 2010 and 2017, respectively. The effects of sea ice  
378 and freshwater discharge changes combined in an approximately additive manner (Figs. 8, 9).  
379 When the forcing from sea ice cover and freshwater discharge were set to be zero in 2010 and  
380 2017, NPP in 2017 was were still 20% smaller than the 2010. This illustrates the importance of  
381 other factors for NPP like wind, cloud cover and inflow to the bay.



## 382 4 Discussion

383 Primary productivity is an essential ecosystem service that shapes the structure of the marine  
384 ecosystem and fuels higher trophic levels such as fish that is vital for the Greenlandic society. It  
385 is therefore important to estimate potential outcomes for primary production under the continued  
386 warming and subsequent ice melt. For the coastal ocean, especially around Greenland, it is  
387 imperative to quantify how changes in sea ice cover and run-off combine to determine the  
388 availability of the two key resources, light and nitrate, determining the magnitude and phenology  
389 of primary production. Sea ice cover and run-off influence light and nitrate availability through  
390 several intermediate processes and their peak impact often occurs in different areas and in  
391 different months. The spatial-temporal variability and complexity of processes involved requires  
392 an approach where detailed *in situ* observations are combined with remote sensing and  
393 modelling. The present study is to our knowledge the first attempt to apply this approach for  
394 coastal Greenland.

395 Our model results show that reduction in spring sea ice cover changes the plankton phenology  
396 but also increases the magnitude of annual production in Disko Bay. This suggests that there is a  
397 replenishment of nitrate into the photic zone to sustain the continued productivity beyond the  
398 initial depletion following the spring bloom. Part of the nitrate input is coupled to the run-off, but  
399 the high modelled productivity from April to July, when liquid run-off is limited suggest that  
400 vertical mixing fueled by wind and tide is important. That less sea ice cover will lead to  
401 increased NPP is in agreement with other studies from the open Arctic areas (Arrigo and van  
402 Dijken, 2015; Vernet et al., 2021). In other Greenland fjords, the turbulence driving vertical  
403 mixing has been shown to be very low (Bendtsen et al., 2021; Randelhoff et al., 2020), but is  
404 seems likely that the open Disko Bay with a tidal amplitude of up to 3 m (Thyrring et al., 2021)  
405 could have an efficient vertical flux of nitrate into the photic zone.

406 Our study site was chosen because the Disko Bay in mid-west Greenland is considered a hot-spot  
407 for marine biodiversity and fisheries, and because it is an area where both sea ice cover and  
408 glacial run-off are likely to be important for productivity. But regional variability is high across  
409 the coastal ocean around Greenland. For example, ice cover is very limited in most of SW  
410 Greenland and is unlikely to drive changes in future primary production, whereas glacial run-off  
411 is less in NE Greenland compared to the rest of Greenland. Furthermore, the dominance of land



412 or marine terminating glaciers as in Disko Bay will be important for the outcome of increased  
413 glacial run-off on individual fjord scale (Hopwood et al., 2020; Lydersen et al., 2014). Finally,  
414 winter concentration of nitrate and vertical gradients in summer differ between the East and West  
415 coast, with low nitrate content in the East Greenland Current generally causing lower  
416 productivity compared to West Greenland (Vernet et al. 2021).

#### 417 **4.1 Phenology of primary producers**

418 A main advantage of the model is that it allows us to estimate the productivity with a higher  
419 temporal and spatial resolution than would be possible from measurements alone. The sea ice  
420 cover had a clear effect on the spring NPP. When sea ice cover is low, spring NPP is starting  
421 earlier compared to years with high sea ice cover, and the largest variation in NPP between years  
422 is seen in the spring months (Fig. 3). The performed scenarios support the importance of sea ice  
423 cover, i.e. the absence of sea ice leads to a considerable increase in the annual NPP on bay scale  
424 (Fig. 9). Potentially, NPP could start as early as February if considering the light availability.  
425 However, for NPP to increase would also require the water column to stabilize, i.e. wind mixing  
426 would need to be sufficiently low (Tremblay et al., 2015). In contrast, the timing of the formation  
427 of the sea ice in fall is not important for the primary productivity, since the sea ice in Disko Bay  
428 does not form before the light has largely disappeared. This is in contrast to high Arctic systems  
429 where sea ice normally forms earlier and a delay in the formation of sea ice in fall may result in  
430 autumn blooms (Ardyna et al., 2014).

#### 431 **4.2 Spatial distribution of NPP**

432 In our analysis, we see a positive effect of the freshwater discharge on the primary productivity  
433 locally and during the summer months. This effect is related to the upwelling that is enhanced by  
434 the freshwater discharge (Fig. C2, C3). The nutrient concentration in the discharge (1.25  $\mu\text{M}$ ,  
435 Hopwood et al., 2020) is lower than the average concentration in the upper 30 m during summer  
436 at the station near the glacier (e.g.  $\sim 4 \mu\text{M NO}_3$ ) (Fig. 7), and will therefore not lead to increased  
437 NPP. This is in accordance with the general picture from glacial affected environments. River  
438 discharge may on the other hand carry higher nutrient concentrations, particularly of nitrogen  
439 (Hopwood et al., 2019).

440 We used two approaches to evaluate the spatial scale of the effect freshwater discharge. The  
441 correlation analyses using salinity as a proxy for the discharge (Fig. 7) suggest that the discharge





442 may influence ~50 km away from the source. The scenarios where we alter the discharge  
443 suggest that the effect is only a couple of percent considering NPP on the Bay scale, whereas on  
444 a more local scale near the glacier the importance is higher (-64% to 147%, Fig. 8 and 9). In the  
445 Godthåbsfjord, which is situated further south at the west coast of Greenland it was found that 1-  
446 11% of the NPP in the Fjord systems is supported by entrainment of N by the three marine  
447 terminating glaciers (Meire et al., 2017). However, considering only the parts of the fjord  
448 directly impacted by the discharge the estimate were 3 times higher (Hopwood et al., 2020).  
449 Analyses from Svalbard fjords impacted showed positive spatiotemporal associations of  
450 chlorophyll a with glacier runoff for 7 out of 14 primary hydrological regions but only within 10  
451 km distance from the shore (Dunse et al., 2022).

452 The modelling in this study allows us to evaluate the combined effect of changes in sea cover  
453 and freshwater discharge in the coastal ecosystem of the Disko Bay. Importantly, this study also  
454 illustrates that within the Arctic coastal zone, the combination of different climate change effects  
455 may lead to different responses within relatively small distances. Thus, while we can suggest a  
456 general increasing trend in the NPP, this may not be evident when considering local  
457 observations. This is important to consider when planning and evaluating field investigations.

#### 458 **4.3 Modelled NPP versus other estimates**

459 The biogeochemical model was validated using all available observations. These are all  
460 concentrations (nutrients) or standing stocks (phytoplankton, zooplankton). The satisfactory  
461 validation is an indication that the rates are also adequately described. Still, it is desirable also to  
462 have direct comparison with rate measurements. There are no available NPP measurements for  
463 our modelling period. However, data are available from 1973-1975 (Andersen, 1981) and  
464 1996/97 (Levinsen and Nielsen, 2002) and 2003 (Sejr et al., 2007). The data from 1996/97 were  
465 *in situ* bottle incubations in the upper 30 m, and no further information on methodology was  
466 given (referred to as unpublished). The sea ice cover was generally high in Disko Bay at that  
467 time (Fig. 4) and we therefore compare the seasonal development to our model estimates from  
468 2017, a year with extensive sea ice cover. The estimate of the annual production from 1996/97  
469 was 28 gC m<sup>-2</sup> d<sup>-1</sup> less than half the estimate from 1970s of 70 gC m<sup>-2</sup> d<sup>-1</sup>, and the modeling  
470 estimates from 2017 of 82 gC m<sup>-2</sup> d<sup>-1</sup> at the same station. The measurements do, however, both  
471 agree with the model on the seasonal timing of NPP with an increase in NPP between March and



472 April, and the Pearson correlation coefficients between measurements and model results were  
473 0.84,  $p < 0.001$  (1996/7) and 0.69,  $p < 0.05$  (1973-75). Data from 2003 (Sejr et al., 2007) are from a  
474 shallow cove only in two shorter periods, but the production of  $195 \text{ mgC m}^{-2} \text{ d}^{-1}$  in April aligns  
475 well with our estimates, whereas the value in September  $27 \text{ mgC m}^{-2} \text{ d}^{-1}$  is somewhat lower.

476 Average estimates of NPP from Arctic glacial fjords with marine terminating glaciers are  
477 reported to be  $400\text{-}800 \text{ mg-C m}^{-2} \text{ d}^{-1}$  during July to September (Hopwood et al., 2020). In the  
478 Arctic Ocean, shelf regions estimates from satellite observations are  $400\text{-}1400 \text{ mgC m}^{-2} \text{ d}^{-1}$  in  
479 April to September during 1998 to 2006 (Pabi et al., 2008). Thus, overall, our model estimates of  
480 NPP in Disko Bay of  $378\text{-}815 \text{ mgC m}^{-2} \text{ d}^{-1}$  between April and September (Fig. 3) are in the same  
481 range as other estimates.

482 In another modelling study, a physically-biologically coupled, regional 3D ocean model  
483 (SINMOD) was compared with ocean color remote sensing (OCRS). Both OCRS and SINMOD  
484 provided similar estimates of the timing and rates of productivity in of the shelves around  
485 Greenland (Vernet et al., 2021). In the region including Disko Bay, the modelled NPP was  
486 generally suggested to be much lower ( $20\text{-}23 \text{ gC m}^{-2} \text{ yr}^{-1}$ ) than our estimate ( $90\text{-}147 \text{ gC m}^{-2} \text{ yr}^{-1}$ )  
487 and the bloom was suggested to generally start later (late May). However, their model mainly  
488 covered the shelf area north of Disko Bay and did not resolve the plume outside the ice fjord.  
489 Moreover, the estimates from OCRS ( $50 \text{ gC m}^{-2} \text{ yr}^{-1}$ ) were about double the modelled values,  
490 and furthermore could only be recorded after ice break-up when the bloom was already on its  
491 maximum (Vernet et al., 2021), suggesting that it could be much higher.

#### 492 **4.4 Uncertainty and potential model improvement**

493 We model the impact of turbidity on light conditions in the water column as a simple relationship  
494 between salinity and light attenuation. More sophisticated light models may be applied in future  
495 models (Murray et al., 2015). However, in a relatively open water system like Disko Bay, the  
496 effect of increased light attenuation due to increased turbidity is only expected within 5-10  
497 kilometers of the glacial outlet. Moreover, we do not expect an impact on the total NPP in the  
498 bay since the nutrients will anyway be used within the bay. A comparison between the spatial  
499 distribution of surface Chl *a* assessed by satellite and the model showed a significant correlation  
500 and the model performance were evaluated good to excellent (Table 3). Still, visual inspections  
501 of the two maps suggest that the effect of the discharge on the Chl *a* spatial distribution were



502 more local and concentrated in the model than what is suggested by the satellite estimates (Fig.  
503 C1). Thus, a higher precision in the spatial distribution of the phytoplankton may be achieved by  
504 improving the model parametrization of light attenuation, e.g. by inserting a passive tracer  
505 reflecting the turbidity in melt water.

506 The uncertainty in the different fresh water discharge source may impact our estimates of marine  
507 productivity differently. Liquid runoff uncertainty and errors are more likely to be random than  
508 bias, and when averaged together (over large spatial areas or times) the uncertainty is reduced  
509 (Mankoff et al., 2020b). Conversely, solid ice discharge uncertainty is comes primarily from  
510 unknown ice thickness, which is time-invariant and therefore must be treated as a bias term  
511 (Mankoff et al., 2020a). It does not reduce when averaged in space or time.

512 We do not specifically model the subglacial discharge of freshwater from the marine terminating  
513 glaciers or from the numerous large icebergs in the bay. Instead, the freshwater discharge was  
514 distributed equally across the upper 100 m in the locations where marine terminating glaciers  
515 were present. Thus, our model is not currently able to resolve the small-scale mixing between  
516 sub-glacial discharge and ambient fjord water in the plume directly in front of the glacier. A  
517 study from another Greenland fjord suggests efficient mixing near the glacial terminus, which  
518 means that the freshwater fraction in the surface water near the glacial front is only 5-7%, which  
519 indicates that the mixing ratio between sub-glacial discharge and fjord water is 1 liter of  
520 meltwater to 13-16 liters of fjord water (Mortensen et al., 2020). The capacity of buoyancy  
521 driven upwelling of subglacial discharge to supply nutrients to the photic zone depends on  
522 several factors including the depth of the freshwater input and the density and nutrient content of  
523 the ambient fjord water. Our approach to distribute the freshwater input in the upper 100 m is a  
524 first attempt to simulate the average conditions across the study area. We were able to reproduce  
525 the general pattern of upwelling (Fig C2+C3) and spatial dynamics of productivity, but the  
526 magnitude could be underestimated. Models of high spatial and process resolution are mainly  
527 developed to describe the transports of heat and salt to glacial ice, in order to estimate the melt  
528 (Burchard et al., 2022). If the focus is to describe the fine scale processes in front of the glacier,  
529 the development within these models may in the future be implemented in ocean models.



#### 530 **4.5 Conclusions**

531 Two important drivers of changes in the Arctic coastal ecosystems are sea ice cover and glacial  
532 freshwater discharge. This modelling study estimates the response of the pelagic net primary  
533 (NPP) production to changes in sea ice cover and freshwater run-off in Disko Bay, West  
534 Greenland, from 2004 to 2018. The difference in annual production between the year with lowest  
535 and highest annual NPP was 63%. Our analysis suggests that sea ice cover was the more  
536 important of the two drivers of annual NPP through its effect on spring timing and annual  
537 production. Fresh water discharge, on the other hand, had a strong impact on the summer NPP  
538 near to the glacial outlet. Hence decreasing ice cover and more discharge can work  
539 synergistically and increase productivity of the coastal ocean around Greenland.

#### 540 **5 Author contribution**

541 EFM, MAM, MS conceptualized the study. MAM, JL, EFM was responsible for the FLEXSEM  
542 development and validation, MHR for HYCOM-CICE, PW for the Arctic 'A20' model, KM for  
543 MAR/ RACMO, and AC for the remote sensing data. MAM and EFM analyzed, synthesized and  
544 visualized the data. EFM prepared the initial draft, and all authors contributed to review and  
545 editing.

#### 546 **6 Competing interests**

547 The authors declare that they have no conflict of interest.

#### 548 **7 Acknowledgements**

549 This research has been supported by the Programme for Monitoring of the Greenland Ice Sheet  
550 (PROMICE) and the European Union's Horizon 2020 research and innovation program  
551 (INTAROS, grant no. 727890), and the Danish Environmental Protection Agency (MST-113  
552 00095 and j-nr 2019 - 8443). MHR was funded by the Danish State through the National Centre  
553 for Climate Research. PW was funded by the Joint Programming Initiative Healthy and  
554 Productive Seas and Oceans (JPI Oceans) project CE2COAST and the EU Horizons 2020 project  
555 FutureMARES, and used resources provided by the Norwegian Metacenter for Computational  
556 Science and Storage Infrastructure (Notur/Norstore projects nn9490k, nn9630k, and ns9630k).  
557 Data from the Greenland Ecosystem Monitoring Programme were provided by the Department



558 of Bioscience, Aarhus University, Denmark, in collaboration with the Department of  
559 Geosciences and Natural Resource Management, Copenhagen University, Denmark. The authors  
560 are solely responsible for all results and conclusions presented, and they do not necessary reflect  
561 the position of the Danish Ministry of the Environment or the Greenland Government.



## 562 **References**

- 563 Andersen, O. G. N.: The annual cycle of phytoplankton primary production and hydrography in  
564 the Disko Bugt area, West Greenland., *Meddelelser om Gronland, Biosci.*, 6, 1981.
- 565 von Appen, W. J., Waite, A. M., Bergmann, M., Bienhold, C., Boebel, O., Bracher, A., Cisewski,  
566 B., Hagemann, J., Hoppema, M., Iversen, M. H., Konrad, C., Krumpen, T., Lochthofen, N.,  
567 Metfies, K., Niehoff, B., Nöthig, E. M., Purser, A., Salter, I., Schaber, M., Scholz, D., Soltwedel,  
568 T., Torres-Valdes, S., Wekerle, C., Wenzhöfer, F., Wietz, M. and Boetius, A.: Sea-ice derived  
569 meltwater stratification slows the biological carbon pump: results from continuous observations,  
570 *Nat. Commun.*, 12(1), 1–16, doi:10.1038/s41467-021-26943-z, 2021.
- 571 Ardyna, M., Babin, M., Gosselin, M., Devred, E., Rainville, L. and Tremblay, J.-É.: Recent  
572 Arctic Ocean sea ice loss triggers novel fall phytoplankton blooms, *Geophys. Res. Lett.*, 41(17),  
573 6207–6212, doi:10.1002/2014GL061047, 2014.
- 574 Ardyna, M., Mundy, C. J., Mayot, N., Matthes, L. C., Oziel, L., Horvat, C., Leu, E., Assmy, P.,  
575 Hill, V., Matrai, P. A., Gale, M., Melnikov, I. A. and Arrigo, K. R.: Under-Ice Phytoplankton  
576 Blooms: Shedding Light on the “Invisible” Part of Arctic Primary Production, *Front. Mar. Sci.*,  
577 7(November), 1–25, doi:10.3389/fmars.2020.608032, 2020.
- 578 Arrigo, K. R. and van Dijken, G. L.: Continued increases in Arctic Ocean primary production,  
579 *Prog. Oceanogr.*, 136, 60–70, doi:10.1016/j.pocean.2015.05.002, 2015.
- 580 Bendtsen, J., Rysgaard, S., Carlson, D. F., Meire, L. and Sejr, M. K.: Vertical Mixing in  
581 Stratified Fjords Near Tidewater Outlet Glaciers Along Northwest Greenland, *J. Geophys. Res.*  
582 *Ocean.*, 126(8), 1–15, doi:10.1029/2020JC016898, 2021.
- 583 Bitz, C. M. and Lipscomb, W. H.: An energy-conserving thermodynamic model of sea ice, *J.*  
584 *Geophys. Res. Ocean.*, 104(C7), 15669–15677, doi:10.1029/1999jc900100, 1999.
- 585 Butenschön, M., Clark, J., Aldridge, J. N., Icarus Allen, J., Artioli, Y., Blackford, J., Bruggeman,  
586 J., Cazenave, P., Ciavatta, S., Kay, S., Lessin, G., Van Leeuwen, S., Van Der Molen, J., De  
587 Mora, L., Polimene, L., Saille, S., Stephens, N. and Torres, R.: ERSEM 15.06: A generic model  
588 for marine biogeochemistry and the ecosystem dynamics of the lower trophic levels, *Geosci.*  
589 *Model Dev.*, 9(4), 1293–1339, doi:10.5194/gmd-9-1293-2016, 2016.



- 590 Chassignet, E. P., Hurlburt, H. E., Smedstad, O. M., Halliwell, G. R., Hogan, P. J., Wallcraft, A.  
591 J., Baraille, R. and Bleck, R.: The HYCOM (HYbrid Coordinate Ocean Model) data assimilative  
592 system, *J. Mar. Syst.*, 65(1-4 SPEC. ISS.), 60–83, doi:10.1016/j.jmarsys.2005.09.016, 2007.
- 593 Cohen, J., Zhang, X., Francis, J., Jung, T., Kwok, R., Overland, J., Ballinger, T. J., Bhatt, U. S.,  
594 Chen, H. W., Coumou, D., Feldstein, S., Gu, H., Handorf, D., Henderson, G., Ionita, M.,  
595 Kretschmer, M., Laliberte, F., Lee, S., Linderholm, H. W., Maslowski, W., Peings, Y., Pfeiffer,  
596 K., Rigor, I., Semmler, T., Stroeve, J., Taylor, P. C., Vavrus, S., Vihma, T., Wang, S., Wendisch,  
597 M., Wu, Y. and Yoon, J.: Divergent consensus on Arctic amplification influence on  
598 midlatitude severe winter weather, *Nat. Clim. Chang.*, 10(1), 20–29, doi:10.1038/s41558-019-  
599 0662-y, 2020.
- 600 Collins, N., Theurich, G., DeLuca, C., Suarez, M., Trayanov, A., Balaji, V., Li, P., Yang, W.,  
601 Hill, C. and da Silva, A.: Design and implementation of components in the Earth System  
602 Modeling Framework, *Int. J. High Perform. Comput. Appl.*, 19(3), 341–350,  
603 doi:10.1177/1094342005056120, 2005.
- 604 Dai, A. and Trenberth, K. E.: Estimates of freshwater discharge from continents: Latitudinal and  
605 seasonal variations, *J. Hydrometeorol.*, 3(6), 660–687, doi:10.1175/1525-  
606 7541(2002)003<0660:EOFDFC>2.0.CO;2, 2002.
- 607 Dee, D. P., Uppala, S. M., Simmons, A. J., Berrisford, P., Poli, P., Kobayashi, S., Andrae, U.,  
608 Balmaseda, M. A., Balsamo, G., Bauer, P., Bechtold, P., Beljaars, A. C. M., van de Berg, L.,  
609 Bidlot, J., Bormann, N., Delsol, C., Dragani, R., Fuentes, M., Geer, A. J., Haimberger, L., Healy,  
610 S. B., Hersbach, H., Hólm, E. V., Isaksen, L., Kållberg, P., Köhler, M., Matricardi, M., McNally,  
611 A. P., Monge-Sanz, B. M., Morcrette, J. J., Park, B. K., Peubey, C., de Rosnay, P., Tavolato, C.,  
612 Thépaut, J. N. and Vitart, F.: The ERA-Interim reanalysis: Configuration and performance of the  
613 data assimilation system, *Q. J. R. Meteorol. Soc.*, 137(656), 553–597, doi:10.1002/qj.828, 2011.
- 614 Dunse, T., Dong, K., Aas, K. S. and Stige, L. C.: Regional-scale phytoplankton dynamics and  
615 their association with glacier meltwater runoff in Svalbard, *Biogeosciences*, 19(2), 271–294,  
616 doi:10.5194/bg-19-271-2022, 2022.
- 617 Egbert, G. D. and Erofeeva, S. Y.: Efficient inverse modeling of barotropic ocean tides, *J.*  
618 *Atmos. Ocean. Technol.*, 19(2), 183–204, doi:10.1175/1520-



- 619 0426(2002)019<0183:EIMOBO>2.0.CO;2, 2002.
- 620 Gladish, C. V., Holland, D. M. and Lee, C. M.: Oceanic Boundary Conditions for Jakobshavn  
621 Glacier. Part II: Provenance and Sources of Variability of Disko Bay and Ilulissat Icefjord  
622 Waters, 1990-- 2011, *J. Phys. Oceanogr.*, 45(2003), 33–63, doi:10.1175/JPO-D-14-0045.1, 2015.
- 623 Hansen, B. U., Elberling, B., Humlum, O. and Nielsen, N.: Meteorological trends (1991–2004) at  
624 Arctic Station, Central West Greenland (69°15'N) in a 130 years perspective, *Geogr. Tidsskr. J.*  
625 *Geogr.*, 106(1), 45–55, doi:10.1080/00167223.2006.10649544, 2006.
- 626 Hernes, P. J., Tank, S. E., Sejr, M. K. and Glud, R. N.: Element cycling and aquatic function in a  
627 changing Arctic, *Limnol. Oceanogr.*, 66(S1), S1–S16, doi:10.1002/lno.11717, 2021.
- 628 Hibler, W. D.: A Dynamic Thermodynamic Sea Ice Model, *J. Phys. Oceanogr.*, 9(4),  
629 doi:10.1175/1520-0485(1979)009<0815:adtsim>2.0.co;2, 1979.
- 630 Holding, J. M., Markager, S., Juul-Pedersen, T., Paulsen, M. L., Møller, E. F., Meire, L. and  
631 Sejr, M. K.: Seasonal and spatial patterns of primary production in a high-latitude fjord affected  
632 by Greenland Ice Sheet run-off, *Biogeosciences*, 16(19), doi:10.5194/bg-16-3777-2019, 2019.
- 633 Hopwood, M. J., Carroll, D., Browning, T. J., Meire, L., Mortensen, J., Krisch, S. and  
634 Achterberg, E. P.: Non-linear response of summertime marine productivity to increased  
635 meltwater discharge around Greenland, *Nat. Commun.*, 9(1), doi:10.1038/s41467-018-05488-8,  
636 2018.
- 637 Hopwood, M. J., Carroll, D., Dunse, T., Hodson, A., Holding, J. M., Iriarte, J. L., Ribeiro, S.,  
638 Achterberg, E. P., Cantoni, C., Carlson, D. F., Chierici, M., Clarke, J. S., Cozzi, S., Fransson, A.,  
639 Juul-Pedersen, T., Winding, M. S. and Meire, L.: Review Article: How does glacier discharge  
640 affect marine biogeochemistry and primary production in the Arctic?, *Cryosph. Discuss.*, (June),  
641 1–51, doi:10.5194/tc-2019-136, 2019.
- 642 Hopwood, M. J., Carroll, D., Dunse, T., Hodson, A., Holding, J. M., Iriarte, J. L., Ribeiro, S.,  
643 Achterberg, E. P., Cantoni, C., Carlson, D. F., Chierici, M., Clarke, J. S., Cozzi, S., Fransson, A.,  
644 Juul-Pedersen, T., Winding, M. H. S. and Meire, L.: Review article: How does glacier discharge  
645 affect marine biogeochemistry and primary production in the Arctic?, *Cryosphere*, 14(4), 1347–  
646 1383, doi:10.5194/tc-14-1347-2020, 2020.





- 647 Høyer, J. L., Karagali, I., Dybkjær, G. and Tonboe, R.: Multi sensor validation and error  
648 characteristics of Arctic satellite sea surface temperature observations, *Remote Sens. Environ.*,  
649 121, 335–346, doi:10.1016/j.rse.2012.01.013, 2012.
- 650 Høyer, J. L., Le Borgne, P. and Eastwood, S.: A bias correction method for Arctic satellite sea  
651 surface temperature observations, *Remote Sens. Environ.*, 146, 201–213,  
652 doi:10.1016/j.rse.2013.04.020, 2014.
- 653 Hunke, E. C.: Viscous-Plastic Sea Ice Dynamics with the EVP Model: Linearization Issues, *J.*  
654 *Comput. Phys.*, 170(1), 18–38, doi:10.1006/jcph.2001.6710, 2001.
- 655 Hunke, E. C. and Dukowicz, J. K.: An elastic-viscous-plastic model for sea ice dynamics, *J.*  
656 *Phys. Oceanogr.*, 27(9), 1849–1867, doi:10.1175/1520-  
657 0485(1997)027<1849:AEVPMF>2.0.CO;2, 1997.
- 658 Ji, R., Jin, M. and Varpe, Ø.: Sea ice phenology and timing of primary production pulses in the  
659 Arctic Ocean., *Glob. Chang. Biol.*, 19(3), 734–41, doi:10.1111/gcb.12074, 2013.
- 660 Kjeldsen, K. K., Korsgaard, N. J., Bjørk, A. A., Khan, S. A., Box, J. E., Funder, S., Larsen, N.  
661 K., Bamber, J. L., Colgan, W., Van Den Broeke, M., Siggaard-Andersen, M. L., Nuth, C.,  
662 Schomacker, A., Andresen, C. S., Willerslev, E. and Kjær, K. H.: Spatial and temporal  
663 distribution of mass loss from the Greenland Ice Sheet since AD 1900, *Nature*, 528(7582), 396–  
664 400, doi:10.1038/nature16183, 2015.
- 665 Large, W. G. and Yeager, S. G.: The global climatology of an interannually varying air - Sea  
666 flux data set, *Clim. Dyn.*, 33(2–3), 341–364, doi:10.1007/s00382-008-0441-3, 2009.
- 667 Lavergne, T., Macdonald Sørensen, A., Kern, S., Tonboe, R., Notz, D., Aaboe, S., Bell, L.,  
668 Dybkjær, G., Eastwood, S., Gabarro, C., Heygster, G., Anne Killie, M., Brandt Kreiner, M.,  
669 Lavelle, J., Saldo, R., Sandven, S. and Pedersen, L. T.: Version 2 of the EUMETSAT OSI SAF  
670 and ESA CCI sea-ice concentration climate data records, *Cryosphere*, 13(1), doi:10.5194/tc-13-  
671 49-2019, 2019.
- 672 Leu, E., Mundy, C. J. J., Assmy, P., Campbell, K., Gabrielsen, T. M. M., Gosselin, M., Juul-  
673 Pedersen, T. and Gradinger, R.: Arctic spring awakening - Steering principles behind the  
674 phenology of vernal ice algal blooms, *Prog. Oceanogr.*, 139, 151–170,



- 675 doi:10.1016/j.pocean.2015.07.012, 2015.
- 676 Levinsen, H. and Nielsen, T. G.: The trophic role of marine pelagic ciliates and heterotrophic  
677 dinoflagellates in arctic and temperate coastal ecosystems: A cross-latitude comparison, *Limnol.*  
678 *Oceanogr.*, 47(2), 427–439, doi:10.4319/lo.2002.47.2.0427, 2002.
- 679 Levinsen, H., Nielsen, T. G. and Hansen, B. W.: Annual succession of marine pelagic protozoans  
680 in Disko Bay, West Greenland, with emphasis on winter dynamics, *Mar. Ecol. Prog. Ser.*, 206,  
681 119–134, doi:10.3354/meps206119, 2000.
- 682 Lovejoy, C., Vincent, W. F., Bonilla, S., Roy, S., Martineau, M. J., Terrado, R., Potvin, M.,  
683 Massana, R. and Pedrós-Alió, C.: Distribution, phylogeny, and growth of cold-adapted  
684 picoprasinophytes in arctic seas, *J. Phycol.*, 43(1), 78–89, doi:10.1111/j.1529-  
685 8817.2006.00310.x, 2007.
- 686 Lydersen, C., Assmy, P., Falk-Petersen, S., Kohler, J., Kovacs, K. M., Reigstad, M., Steen, H.,  
687 Strøm, H., Sundfjord, A., Varpe, Ø., Walczowski, W., Weslawski, J. M. and Zajaczkowski, M.:  
688 The importance of tidewater glaciers for marine mammals and seabirds in Svalbard, Norway, *J.*  
689 *Mar. Syst.*, 129, 452–471, doi:10.1016/j.jmarsys.2013.09.006, 2014.
- 690 Maar, M., Møller, E. F., Larsen, J., Madsen, K. S., Wan, Z., She, J., Jonasson, L. and Neumann,  
691 T.: Ecosystem modelling across a salinity gradient from the North Sea to the Baltic Sea, *Ecol.*  
692 *Modell.*, 222(10), 1696–1711, doi:10.1016/j.ecolmodel.2011.03.006, 2011.
- 693 Maar, M., Markager, S., Madsen, K. S., Windolf, J., Lyngsgaard, M. M., Andersen, H. E. and  
694 Møller, E. F.: The importance of local versus external nutrient loads for Chl a and primary  
695 production in the Western Baltic Sea, *Ecol. Modell.*, 320, doi:10.1016/j.ecolmodel.2015.09.023,  
696 2016.
- 697 Madsen, K. S., Rasmussen, T. A. S., Ribergaard, M. H. and Ringgaard, I. M.: High resolution  
698 sea-ice modelling and validation of the Arctic with focus on South Greenland Waters, 2004-  
699 2013, *Polarforschung*, 85(2), 101–105, doi:10.2312/polfor.2016.006, 2016.
- 700 Mankoff, K. D., Straneo, F., Cenedese, C., Das, S. B., Richards, C. G. and Singh, H.: Structure  
701 and dynamics of a subglacial discharge plume in a Greenlandic fjord, *J. Geophys.*  
702 *Res. Ocean.*, 121(12), 8670–8688, doi:10.1002/2016JC011764, 2016.



- 703 Mankoff, K. D., Solgaard, A., Colgan, W., Ahlstrøm, A. P., Abbas Khan, S. and Fausto, R. S.:  
704 Greenland Ice Sheet solid ice discharge from 1986 through March 2020, *Earth Syst. Sci. Data*,  
705 12(2), 1367–1383, doi:10.5194/essd-12-1367-2020, 2020a.
- 706 Mankoff, K. D., Ahlstrøm, A. P., Colgan, W., Faust, R. S., Fettweis, X., Kondo, K., Langley, K.,  
707 Noël, B., Sugiyama, S. and As, D. van: Greenland liquid water runoff from 1979 through 2017,  
708 *Earth Syst. Sci. Data*, (April), doi:doi.org/10.5194/essd-2020-47, 2020b.
- 709 Mankoff, K. D., Fettweis, X., Langen, P. L., Stendel, M., Kjeldsen, K. K., Karlsson, N. B., Noël,  
710 B., van den Broeke, M. R., Solgaard, A., Colgan, W., Box, J. E., Simonsen, S. B., King, M. D.,  
711 Ahlstrøm, A. P., Andersen, S. B. and Fausto, R. S.: Greenland ice sheet mass balance from 1840  
712 through next week, *Earth Syst. Sci. Data*, 13(10), 5001–5025, doi:10.5194/essd-13-5001-2021,  
713 2021.
- 714 Massicotte, P., Peeken, I., Katlein, C., Flores, H., Huot, Y., Castellani, G., Arndt, S., Lange, B.  
715 A., Tremblay, J.-É. and Babin, M.: Sensitivity of phytoplankton primary production estimates to  
716 available irradiance under heterogeneous sea-ice conditions, *J. Geophys. Res. Ocean.*, (June),  
717 doi:10.1029/2019JC015007, 2019.
- 718 Meier, W. N., Hovelsrud, G. K., van Oort, B. E. H., Key, J. R., Kovacs, K. M., Michel, C., Haas,  
719 C., Granskog, M. A., Gerland, S., Perovich, D. K., Makshtas, A. and Reist, J. D.: Arctic sea ice  
720 in transformation: A review of recent observed changes and impacts on biology and human  
721 activity, *Rev. Geophys.*, 52(3), 185–217, doi:10.1002/2013RG000431, 2014.
- 722 Meire, L., Mortensen, J., Meire, P., Juul-Pedersen, T., Sejr, M. K., Rysgaard, S., Nygaard, R.,  
723 Huybrechts, P. and Meysman, F. J. R.: Marine-terminating glaciers sustain high productivity in  
724 Greenland fjords, *Glob. Chang. Biol.*, 23(12), 5344–5357, doi:10.1111/gcb.13801, 2017.
- 725 Menden-Deuer, S., Lawrence, C. and Franzè, G.: Herbivorous protist growth and grazing rates at  
726 in situ and artificially elevated temperatures during an Arctic phytoplankton spring bloom, *PeerJ*,  
727 2018(7), doi:10.7717/peerj.5264, 2018.
- 728 Møller, E. F. and Nielsen, T. G.: Borealization of Arctic zooplankton — smaller and less fat  
729 zooplankton species in Disko Bay , Western Greenland , , 1–14, doi:10.1002/lno.11380, 2019.
- 730 Møller, E. F. and Nielsen, T. G.: Borealization of Arctic zooplankton—smaller and less fat



- 731 zooplankton species in Disko Bay, Western Greenland, *Limnol. Oceanogr.*, 65(6), 1175–1188,  
732 doi:10.1002/lno.11380, 2020.
- 733 Møller, E. F. E. F., Maar, M., Jónasdóttir, S. H. S. H., Gissel Nielsen, T. and Tönnesson, K.: The  
734 effect of changes in temperature and food on the development of *Calanus finmarchicus* and  
735 *Calanus helgolandicus* populations, *Limnol. Oceanogr.*, 57(1), 211–220,  
736 doi:10.4319/lno.2012.57.1.0211, 2012.
- 737 Møller, E. F. E. F., Bohr, M., Kjellerup, S., Maar, M., Møhl, M., Swalethorp, R. and Nielsen, T.  
738 G. T. G.: *Calanus finmarchicus* egg production at its northern border, *J. Plankton Res.*, 38(5),  
739 1206–1214, doi:10.1093/plankt/fbw048, 2016.
- 740 Morlighem, M., Williams, C. N., Rignot, E., An, L., Arndt, J. E., Bamber, J. L., Catania, G.,  
741 Chauché, N., Dowdeswell, J. A., Dorschel, B., Fenty, I., Hogan, K., Howat, I., Hubbard, A.,  
742 Jakobsson, M., Jordan, T. M., Kjeldsen, K. K., Millan, R., Mayer, L., Mouginot, J., Noël, B. P.  
743 Y., O’Cofaigh, C., Palmer, S., Rysgaard, S., Seroussi, H., Siegert, M. J., Slabon, P., Straneo, F.,  
744 van den Broeke, M. R., Weinrebe, W., Wood, M. and Zinglensen, K. B.: BedMachine v3:  
745 Complete Bed Topography and Ocean Bathymetry Mapping of Greenland From Multibeam  
746 Echo Sounding Combined With Mass Conservation, *Geophys. Res. Lett.*, 44(21), 11,051–11,061,  
747 doi:10.1002/2017GL074954, 2017.
- 748 Mortensen, J., Rysgaard, S., Bendtsen, J., Lennert, K., Kanzow, T., Lund, H. and Meire, L.:  
749 Subglacial Discharge and Its Down-Fjord Transformation in West Greenland Fjords With an Ice  
750 Mélange, *J. Geophys. Res. Ocean.*, 125(9), 1–13, doi:10.1029/2020JC016301, 2020.
- 751 Mouginot, J., Rignot, E., Bjørk, A. A., van den Broeke, M., Millan, R., Morlighem, M., Noël, B.,  
752 Scheuchl, B. and Wood, M.: Forty-six years of Greenland Ice Sheet mass balance from 1972 to  
753 2018, *Proc. Natl. Acad. Sci. U. S. A.*, 116(19), 9239–9244, doi:10.1073/pnas.1904242116, 2019.
- 754 Murray, C., Markager, S., Stedmon, C. A., Juul-Pedersen, T., Sej, M. K. and Bruhn, A.: The  
755 influence of glacial melt water on bio-optical properties in two contrasting Greenlandic fjords,  
756 *Estuar. Coast. Shelf Sci.*, 163(PB), 72–83, doi:10.1016/j.ecss.2015.05.041, 2015.
- 757 Neumann, T.: Towards a 3D-ecosystem model of the Baltic Sea, *J. Mar. Syst.*, 25(3–4), 405–  
758 419, doi:10.1016/S0924-7963(00)00030-0, 2000.



- 759 Pabi, S., van Dijken, G. L. and Arrigo, K. R.: Primary production in the Arctic Ocean, 1998-  
760 2006, *J. Geophys. Res. Ocean.*, 113(8), 1998–2006, doi:10.1029/2007JC004578, 2008.
- 761 Randelhoff, A., Holding, J., Janout, M., Sejr, M. K., Babin, M., Tremblay, J.-éric, Alkire, M. B.  
762 and Oliver, H.: Pan-Arctic Ocean Primary Production Constrained by Turbulent Nitrate Fluxes, ,  
763 7(March), 1–15, doi:10.3389/fmars.2020.00150, 2020.
- 764 Rasmussen, T. A. S., Høyer, J. L., Ghent, D., Bulgin, C. E., Dybkjær, G., Ribergaard, M. H.,  
765 Nielsen-Englyst, P. and Madsen, K. S.: Impact of Assimilation of Sea-Ice Surface Temperatures  
766 on a Coupled Ocean and Sea-Ice Model, *J. Geophys. Res. Ocean.*, 123(4), 2440–2460,  
767 doi:10.1002/2017JC013481, 2018.
- 768 Rysgaard, S., Boone, W., Carlson, D., Sejr, M. K., Bendtsen, J., Juul-Pedersen, T., Lund, H.,  
769 Meire, L. and Mortensen, J.: An Updated View on Water Masses on the pan-West Greenland  
770 Continental Shelf and Their Link to Proglacial Fjords, *J. Geophys. Res. Ocean.*, 125(2), 0–3,  
771 doi:10.1029/2019JC015564, 2020.
- 772 Sejr, M. K., Nielsen, T. G., Rysgaard, S., Risgaard-petersen, N., Sturluson, M. and Blicher, M.  
773 E.: Fate of pelagic organic carbon and importance of pelagic – benthic coupling in a shallow  
774 cove, *Mar. Ecol. Prog. Ser.*, 341, 75–88, 2007.
- 775 Shchepetkin, A. F. and McWilliams, J. C.: The regional oceanic modeling system (ROMS): A  
776 split-explicit, free-surface, topography-following-coordinate oceanic model, *Ocean Model.*, 9(4),  
777 347–404, doi:10.1016/j.ocemod.2004.08.002, 2005.
- 778 Steele, M., Morley, R. and Ermold, W.: PHC: A global ocean hydrography with a high-quality  
779 Arctic Ocean, *J. Clim.*, 14(9), 2079–2087, doi:10.1175/1520-  
780 0442(2001)014<2079:PAGOHW>2.0.CO;2, 2001.
- 781 Stroeve, J. C., Markus, T., Boisvert, L., Miller, J. and Barrett, A.: Changes in Arctic melt season  
782 and implications for sea ice loss, *Geophys. Res. Lett.*, 41(4), 1216–1225,  
783 doi:10.1002/2013GL058951, 2014.
- 784 Swalethorp, R., Kjellerup, S., Dünweber, M., Nielsen, T., Møller, E., Rysgaard, S. and Hansen,  
785 B.: Grazing, egg production, and biochemical evidence of differences in the life strategies of  
786 *Calanus finmarchicus*, *C. glacialis* and *C. hyperboreus* in Disko Bay, western Greenland, *Mar.*



- 787 Ecol. Prog. Ser., 429, 125–144, doi:10.3354/meps09065, 2011.
- 788 Thomas, D. N., Baumann, M. E. M. and Gleitz, M.: Efficiency of carbon assimilation and  
789 photoacclimation in a small unicellular Chaetoceros species from the Weddell Sea (Antarctica):  
790 influence of temperature and irradiance, *J. Exp. Mar. Bio. Ecol.*, 157(2), 195–209,  
791 doi:10.1016/0022-0981(92)90162-4, 1992.
- 792 Thyrring, J., Wegeberg, S., Blicher, M. E., Krause-Jensen, D., Høgslund, S., Olesen, B., Jozef,  
793 W., Mouritsen, K. N., Peck, L. S. and Sejr, M. K.: Latitudinal patterns in intertidal ecosystem  
794 structure in West Greenland suggest resilience to climate change, *Ecography (Cop.)*, 44(8),  
795 1156–1168, doi:10.1111/ecog.05381, 2021.
- 796 Tremblay, J.-É. and Gagnon, J.: The effects of irradiance and nutrient supply on the productivity  
797 of Arctic waters: a perspective on climate change, in *Influence of Climate Change on the*  
798 *Changing Arctic and Sub-Arctic Conditions*, pp. 73–93, Springer Netherlands, Dordrecht., 2009.
- 799 Tremblay, J. É., Anderson, L. G., Matrai, P., Coupel, P., Bélanger, S., Michel, C. and Reigstad,  
800 M.: Global and regional drivers of nutrient supply, primary production and CO<sub>2</sub> drawdown in  
801 the changing Arctic Ocean, *Prog. Oceanogr.*, 139, 171–196, doi:10.1016/j.pocean.2015.08.009,  
802 2015.
- 803 Vernet, M., Ellingsen, I., Marchese, C., Bélanger, S., Cape, M., Slagstad, D. and Matrai, P. A.:  
804 Spatial variability in rates of Net Primary Production (NPP) and onset of the spring bloom in  
805 Greenland shelf waters, *Prog. Oceanogr.*, 198(September 2020), 102655,  
806 doi:10.1016/j.pocean.2021.102655, 2021.
- 807 Zhang, J., Spitz, Y. H., Steele, M., Ashjian, C., Campbell, R., Berline, L. and Matrai, P.:  
808 Modeling the impact of declining sea ice on the Arctic marine planktonic ecosystem, *J. Geophys.*  
809 *Res. Ocean.*, 115(10), doi:10.1029/2009JC005387, 2010.
- 810 Yang, X., Petersen, C., Amstrup B., Andersen, B. S., Hansen, Feddersen, H., Kmit, M.,  
811 Korsholm, U., Lindberg, K., Mogensen, K., Sass, B.H., Sattler, K., Nielsen, N.W.: The DMI-  
812 HIRLAM upgrade in June 2004. DMI-Tech. Rep. 05-09, Danish Meteorological Institute,  
813 Copenhagen, Denmark, 2005.



814 Yang, X., Palmason, B., Andersen, B. S., Hansen Sass, B., Amstrup, B., Dahlbom, M., Petersen,  
815 C., Pagh Nielsen, K., Mottram, R., Woetmann, N., Mahura, A. Thorsteinsson, S., Nawri, N., and  
816 Petersen, G. N. 2017: IGA, the Joint Operational HARMONIE by DMI and IMO, ALADIN-  
817 HIRLAM Newsletter, No. 8, 87–94, 2017.

818 Yang, X., Palmason, B., Sattler, K., Thorsteinsson, S., Amstrup, B., Dahlbom, M., Hansen Sass,  
819 B., Pagh Nielsen, K., Petersen, G. N. 2018: IGB, the Upgrade to the Joint Operational  
820 HARMONIE by DMI and IMO in 2018, ALADIN-HIRLAM Newsletter, No. 11, 93-96, 2018.

821



822 **8 Tables**

823 Table 1: Characteristics of the reference model runs of 2010 and 2017, and the annual average  
 824 NPP in the bay obtained from scenarios runs with changes in the sea ice cover and the freshwater  
 825 discharge (Figure 8 and 9). SD are the standard variation between the different model grid cells.

				2010	2017
<b>Reference</b>	Average annual primary production	gC m <sup>-2</sup> yr <sup>-1</sup>		147 ±41	90 ±28
	Average annual discharge	m <sup>3</sup> s <sup>-1</sup>		6275	4058
	Average annual sea ice cover, March-April	%		24	79
<b>Scenarios</b>	Average annual primary production	gC m <sup>-2</sup> yr <sup>-1</sup>	No sea ice	150 ±50	120 ±35
			No freshwater discharge	144 ±53	90 ±46
			No sea ice, No freshwater discharge	147 ±47	119 ±32
			2 x freshwater discharge	149 ±48	90 ±45
			No sea ice, 2 x freshwater discharge	152 ±53	122 ±35

826





827 Table 2: Statistics for seasonal comparison between observational data (monthly climatology)  
828 and model data (monthly average from 2005 to 2018) at the Disko Bay Station.  $N=12$  for  
829 copepods,  $N=11$  for temperature, salinity and Chl  $a$  and  $N=10$  for other variables (see Figure 4).  
830 All correlations were significant ( $p<0.01$ ).

831

	Unit	Model error	RMSE	Correlation	$cf$
Temperature	°C	-0.28	0.96	0.94	0.31
Salinity	-	-0.09	0.21	0.79	0.56
NO <sub>3</sub>	mmol m <sup>-3</sup>	0.00	1.43	0.87	0.39
Silicate	mmol m <sup>-3</sup>	0.78	1.70	0.83	0.66
Phosphate	mmol m <sup>-3</sup>	-0.01	0.12	0.82	0.46
Chl $a$	mg m <sup>-3</sup>	0.03	0.97	0.87	0.37
Copepod biomass	mgC m <sup>-3</sup>	0.83	4.66	0.94	0.23

832



833 Table 3: Statistics for the spatial comparison between remote sensing data and surface model  
 834 data for spring (April-June) and summer (July-September) in 2010 and 2017. In spring 2017,  
 835 only June is included due to ice cover in April-May.  $N=6145$ , and all correlations were  
 836 significant ( $p<0.01$ ).

	Model error	RMSE	Correlatio n	<i>cf</i>
<i>Surface temperature</i>				
2010 spring	0.8	1.3	0.45	1.0
2010 summer	-1.4	2.0	0.14	1.5
2017 spring	0.8	1.4	0.58	0.9
2017 summer	-2.0	2.3	0.33	0.2
<i>Log<sub>10</sub> (Chl a [mg/m<sup>3</sup>])</i>				
2010 spring	0.6	0.7	0.30	0.4
2010 summer	0.5	0.8	0.33	0.2
2017 spring	1.7	1.8	0.29	1.7
2017 summer	0.9	1.1	0.46	1.2

837



## 838 9 Figures

839 Figure 1: Map of Disko Bay with the bathymetry, the Flexsem model grid, position of fresh  
840 water sources (red dots: land runoff, red dots with black circle: land + ice runoff), position of two  
841 stations presented in more detail, and the area used for calculation of the average Disko Bay  
842 primary production (red box).

843 Figure 2: Development in freshwater discharge and sea ice cover over time. a) Fresh water  
844 discharge from the Greenland ice sheet divided into liquid from precipitation over land (Land  
845 runoff), liquid deriving from melt from the Greenland Ice sheet/glaciers (Ice runoff) and ice  
846 deriving directly from the glacier (solid ice) 1960 to 2019, and b) number of days with more than  
847 40% sea ice cover from 1986 to 2019, derived from satellite measurement (AICE), by the sea ice  
848 model providing input to the this study (CICE), and by visual observation at Arctic Station,  
849 Qeqertarsuaq (AS).

850 Figure 3: Primary production, sea ice cover and freshwater discharge in Disko Bay from 2004 to  
851 2018. Primary production and sea ice cover are assessed in the red square in Fig 1, whereas the  
852 freshwater discharge are from the full model domain. (a) Average annual primary production ( $\text{gC}$   
853  $\text{m}^{-2} \text{year}^{-1}$ )  $\pm$  SD (variation between model grid cells), (b) the average monthly primary  
854 production ( $\text{mgC m}^{-2} \text{day}^{-1}$ )  $\pm$  SD (variation between years), light is average from Arctic station  
855 (2010-2019), (c) the annual average sea ice cover in March and April (%), (d) the average  
856 monthly sea ice cover (%), (e) the average annual fresh water discharge ( $\text{m}^3 \text{s}^{-1}$ ), and (f) the  
857 average monthly fresh water discharge ( $1000 \text{ m}^3 \text{s}^{-1}$ ).

858 Figure 4: Comparison of monthly means ( $\pm$ SD) of observations and model data (2004-2018) at  
859  $69^{\circ}14'N$ ,  $53^{\circ}23'W$  for (a) temperature ( $^{\circ}\text{C}$ ), (b) salinity, (c) nitrate ( $\text{mmol m}^{-3}$ ), (d) silicate  
860 ( $\text{mmol m}^{-3}$ ), (e) phosphate ( $\text{mmol m}^{-3}$ ), (f) Chl *a*, ( $\text{mg m}^{-3}$ ), (g) microzooplankton biomass ( $\text{mgC}$   
861  $\text{m}^{-3}$ ), and (h) mesozooplankton biomass ( $\text{mgC m}^{-3}$ ). Means are averaged over 0-20 m depth,  
862 except for mesozooplankton which it is 0-50 m.

863 Figure 5: Sea ice cover (%), average nitrate concentration in 0-30 m ( $\text{mmol m}^{-3}$ ) average Chl *a*  
864 concentration in 0-30 m ( $\text{mg m}^{-3}$ ) and primary production ( $\text{mgC m}^{-2} \text{d}^{-1}$ ) at a station in open Bay  
865 (Bay Station) and at one close to the glacier (Glacier Station) (Fig. 1) in 2010 and 2017.



866 Figure 6: Average spatial distribution of primary production ( $\text{gC m}^{-2}$ ) in 2010 and 2017  
867 respectively for the periods A)+D) March-October, B)+E) March-June and C) +F) July-October.

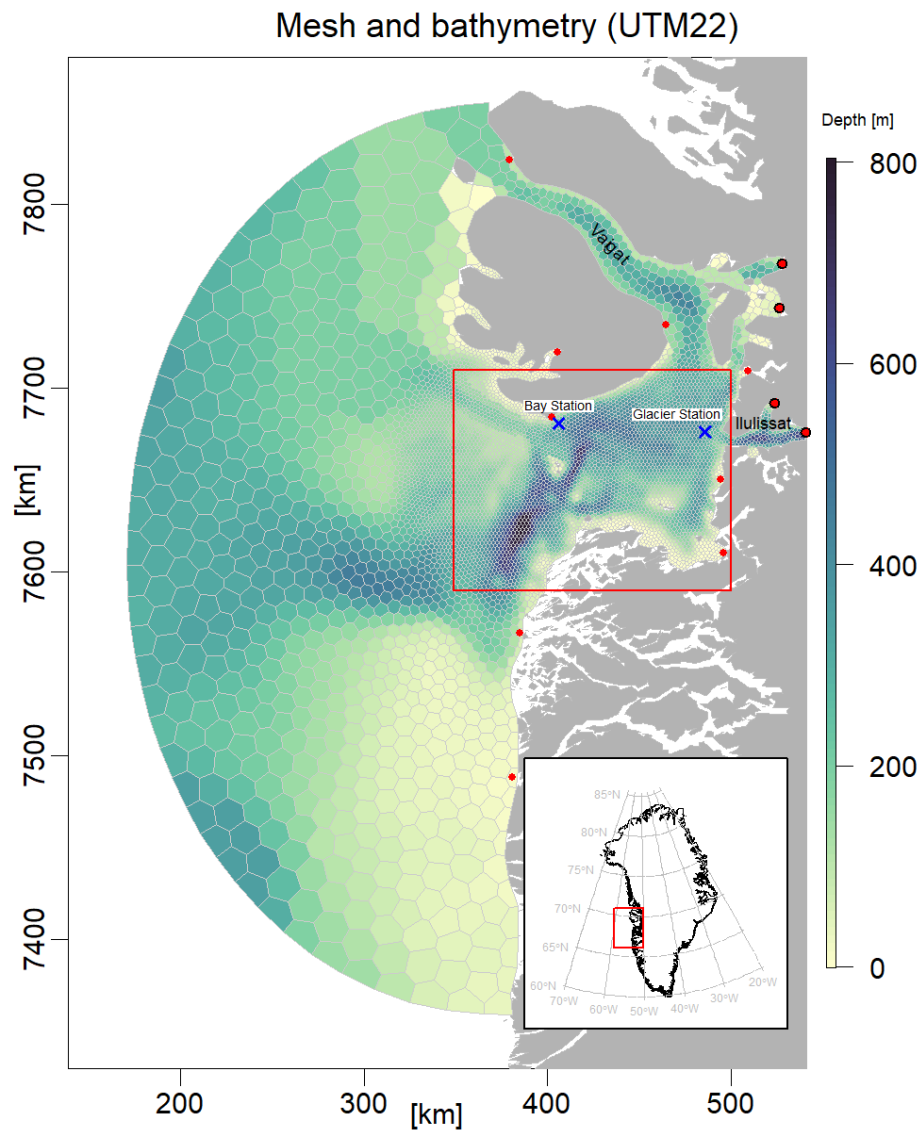
868 Figure 7: Correlation coefficients between the annual primary production (a) and average sea ice  
869 cover in March-April and (b) and surface salinity across the period 2004-2018.

870 Figure 8: Response of the annual primary production to simple scenarios of changes in sea ice  
871 cover and freshwater discharge (Q) in 2010 expressed as percentage change relative to the  
872 standard model run. The percentages in the bottom of the figure are the changes in primary  
873 production in the total area shown. The following model scenarios were run (Table 1): (a)  
874 standard model run, (b) assuming no sea ice cover, (c) assuming no freshwater discharge from  
875 the Greenland ice sheet, (d) the combination of (b) and (c), (e) assuming 2 times the freshwater  
876 discharge of the standard run, and (f) the combination of (b) and (e).

877 Figure 9: Response of the annual primary production to simple scenarios of changes in sea ice  
878 cover and freshwater discharge (Q) in 2017 expressed as percentage change relative to the  
879 standard model run. The percentages in the bottom of the figure are the changes in primary  
880 production in the total area shown. The following model scenarios were run (Table 1): (a)  
881 standard model run, (b) assuming no sea ice cover, (c) assuming no freshwater discharge from  
882 the Greenland ice sheet, (d) the combination of (b) and (c), (e) assuming 2 times the freshwater  
883 discharge of the standard run, and (f) the combination of (b) and (e).



Figure 1: Map of Disko Bay with the bathymetry, the Flexsem model grid, position of fresh water sources (red dots: land runoff, red dots with black circle: land + ice runoff), position of two stations presented in more detail, and the area used for calculation of the average Disko Bay primary production (red box).



884  
885



Figure 2: Development in freshwater discharge and sea ice cover over time. a) Fresh water discharge from the Greenland ice sheet divided into liquid from precipitation over land (Land runoff), liquid deriving from melt from the Greenland Ice sheet/glaciers (Ice runoff) and ice deriving directly from the glacier (solid ice) 1960 to 2019, and b) number of days with more than 40% sea ice cover from 1986 to 2019, derived from satellite measurement (AICE), by the sea ice model providing input to the this study (CICE), and by visual observation at Arctic Station, Qeqertarsuaq (AS).

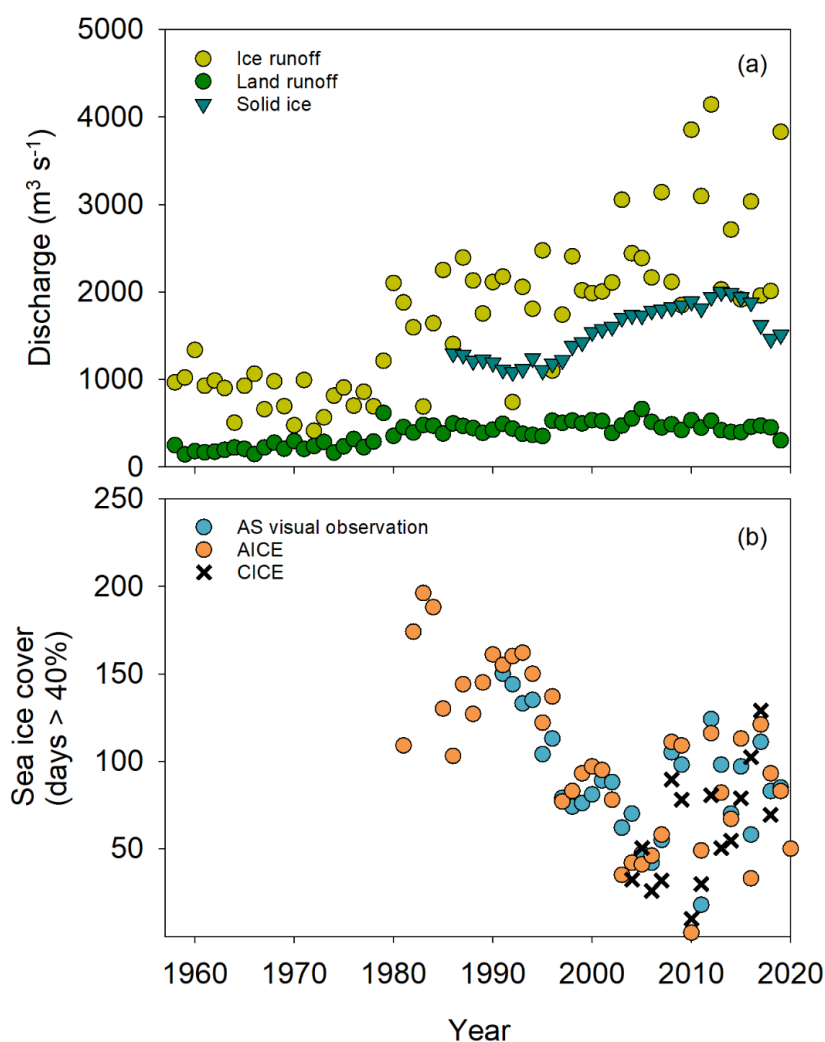




Figure 3: Primary production, sea ice cover and freshwater discharge in Disko Bay from 2004 to 2018. Primary production and sea ice cover are assessed in the red square in Fig 1, whereas the freshwater discharge are from the full model domain. (a) Average annual primary production ( $\text{gC m}^{-2} \text{ year}^{-1}$ )  $\pm$  SD (variation between model grid cells), (b) the average monthly primary production ( $\text{mgC m}^{-2} \text{ day}^{-1}$ )  $\pm$  SD (variation between years), light is average from Arctic station (2010-2019), (c) the annual average sea ice cover in March and April (%), (d) the average monthly sea ice cover (%), (e) the average annual fresh water discharge ( $\text{m}^3 \text{ s}^{-1}$ ), and (f) the average monthly fresh water discharge ( $1000 \text{ m}^3 \text{ s}^{-1}$ ).

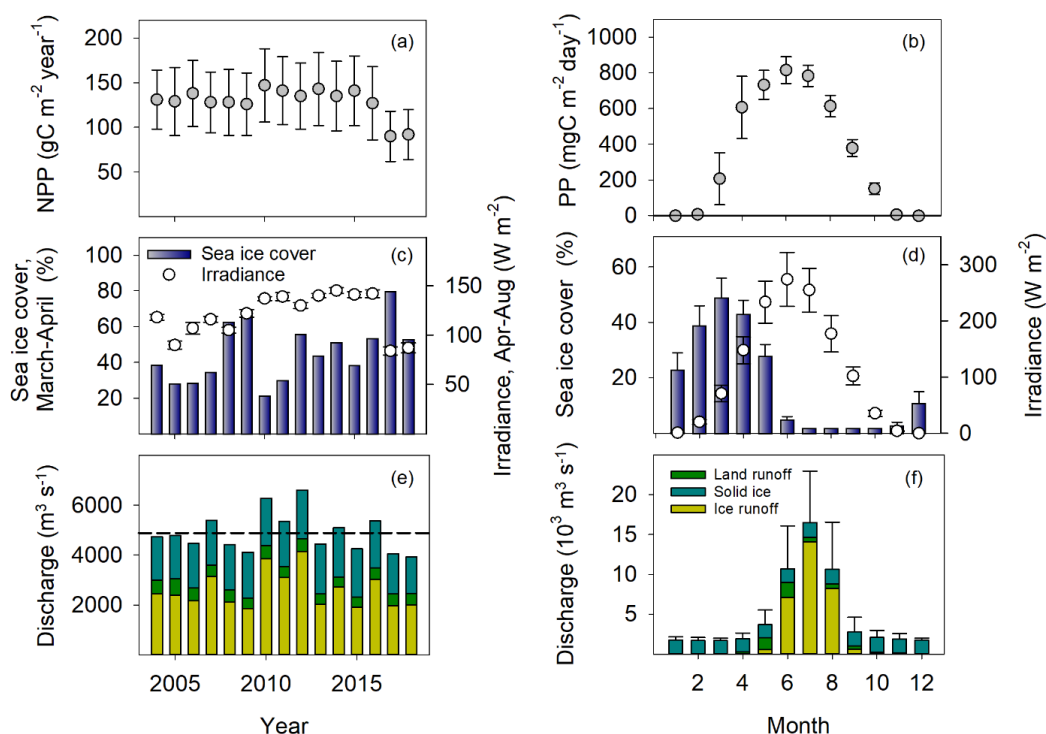
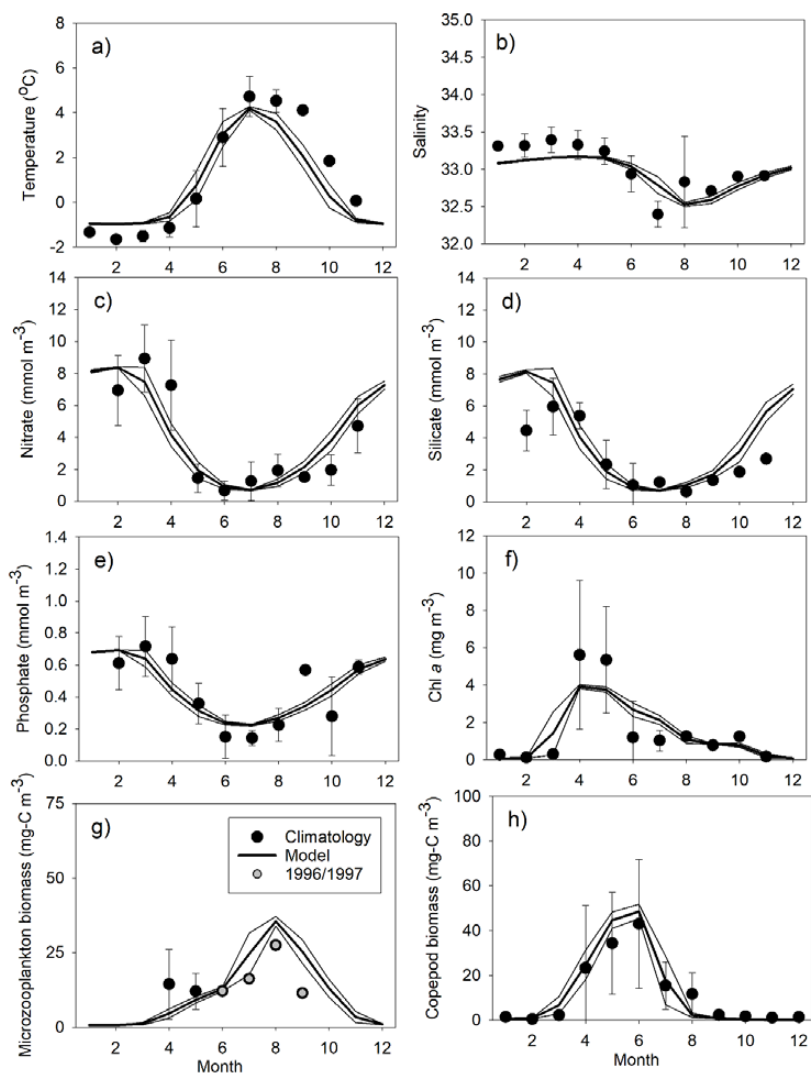




Figure 4: Comparison of monthly means ( $\pm$ SD) of observations and model data (2004-2018) at  $69^{\circ}14'N$ ,  $53^{\circ}23'W$  for (a) temperature ( $^{\circ}C$ ), (b) salinity, (c) nitrate ( $mmol\ m^{-3}$ ), (d) silicate ( $mmol\ m^{-3}$ ), (e) phosphate ( $mmol\ m^{-3}$ ), (f) Chl *a*, ( $mg\ m^{-3}$ ), (g) microzooplankton biomass ( $mgC\ m^{-3}$ ), and (h) mesozooplankton biomass ( $mgC\ m^{-3}$ ). Means are averaged over 0-20 m depth, except for mesozooplankton which it is 0-50 m.



888

889





890

Fig 5: Sea ice cover (%), average nitrate concentration in 0-30 m ( $\text{mmol m}^{-3}$ ) average Chl *a* concentration in 0-30 m ( $\text{mg m}^{-3}$ ) and primary production ( $\text{mgC m}^{-2} \text{d}^{-1}$ ) at a station in open Bay (Bay Station) and at one close to the glacier (Glacier Station) (Fig. 1) in 2010 and 2017.

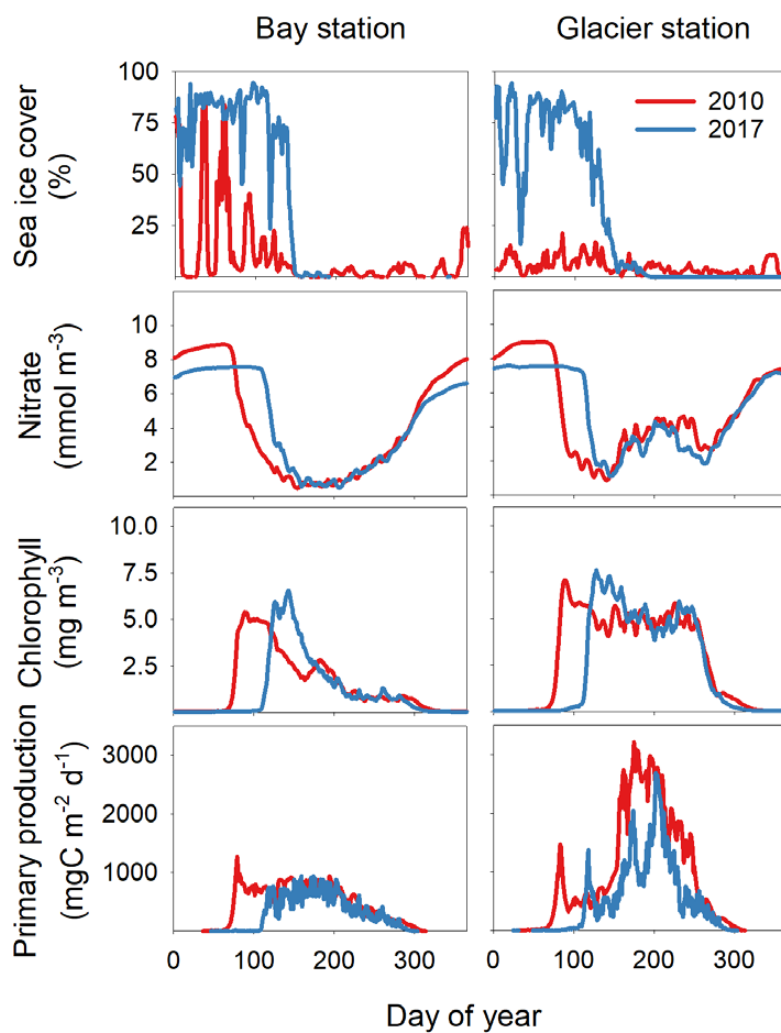




Fig 6: Average spatial distribution of primary production ( $\text{gC m}^{-2}$ ) in 2010 and 2017 respectively for the periods A)+D) March-October, B)+E) March-June and C) +F) July-October.

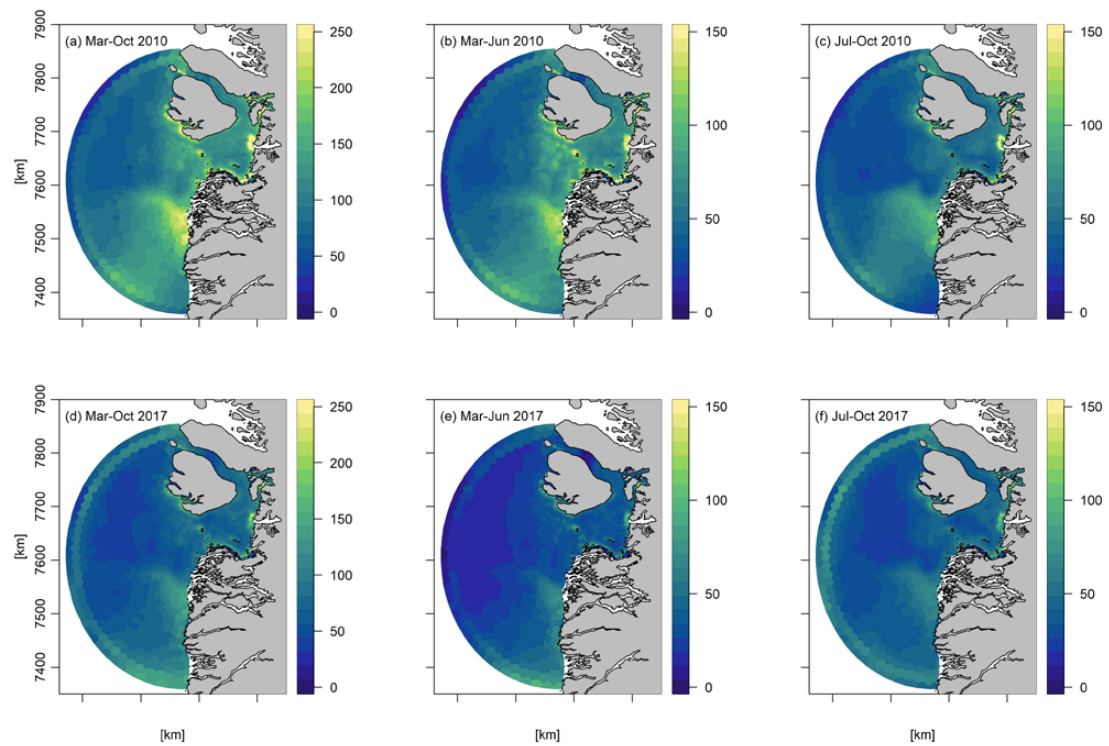
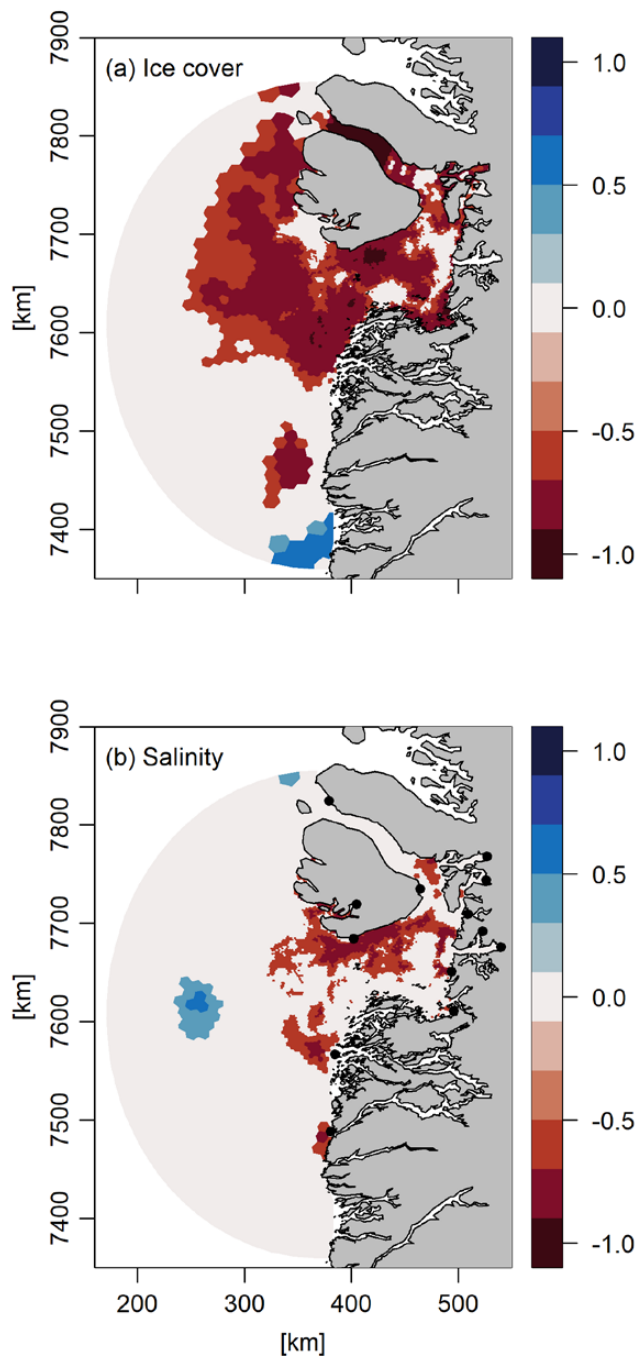




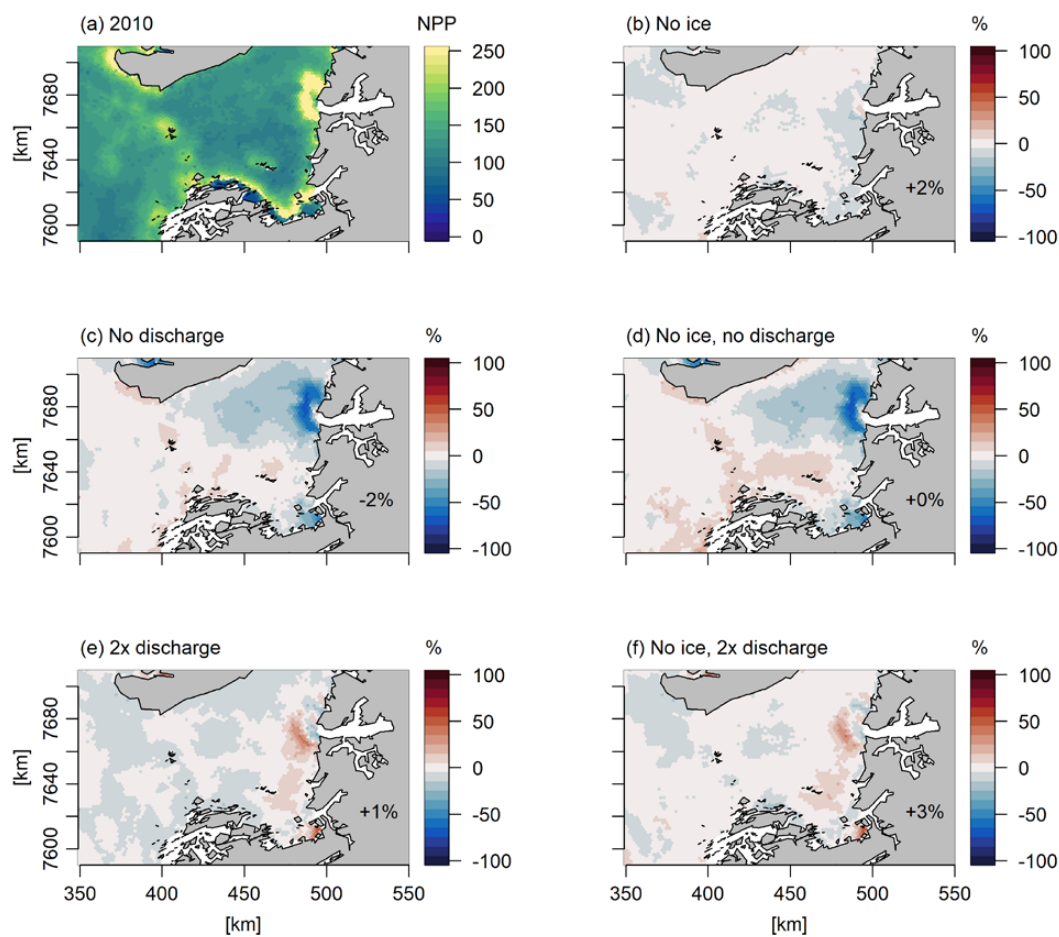
Fig 7: Correlation coefficients between the annual primary production (a) and average sea ice cover in March-April and (b) and surface salinity across the period 2004-2018.





891

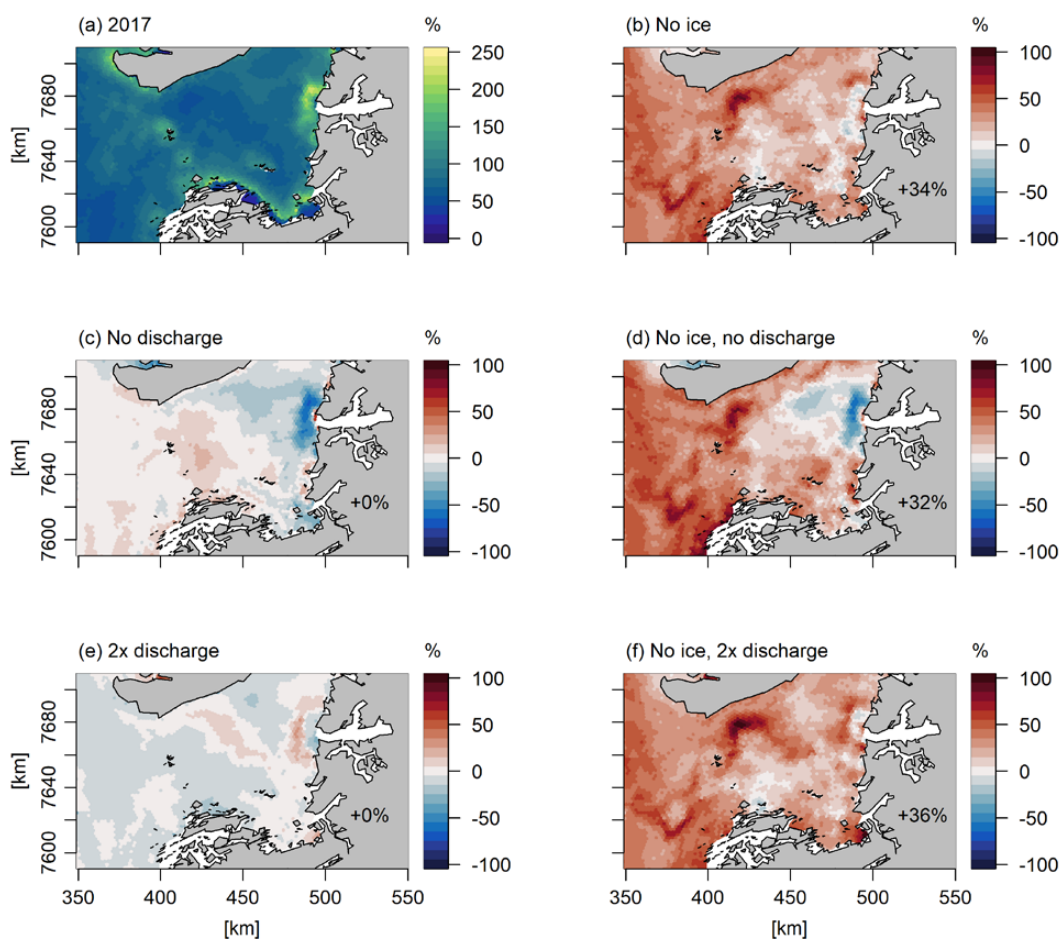
Fig 8: Response of the annual primary production to simple scenarios of changes in sea ice cover and freshwater discharge (Q) in 2010 expressed as percentage change relative to the standard model run. The percentages in the bottom of the figure are the changes in primary production in the total area shown. The following model scenarios were run (Table 1): (a) standard model run, (b) assuming no sea ice cover, (c) assuming no freshwater discharge from the Greenland ice sheet, (d) the combination of (b) and (c), (e) assuming 2 times the freshwater discharge of the standard run, and (f) the combination of (b) and (e).



892



Fig 9: Response of the annual primary production to simple scenarios of changes in sea ice cover and freshwater discharge (Q) in 2017 expressed as percentage change relative to the standard model run. The percentages in the bottom of the figure are the changes in primary production in the total area shown. The following model scenarios were run (Table 1): (a) standard model run, (b) assuming no sea ice cover, (c) assuming no freshwater discharge from the Greenland ice sheet, (d) the combination of (b) and (c), (e) assuming 2 times the freshwater discharge of the standard run, and (f) the combination of (b) and (e).





894 10 Appendices

895 **10.1 Appendix A, Ecological model constants**

896 Table A.1. Constants in the FlexSem ecological Disko Bay model.

Parameter	Description	Numerical value	Units
<b>Phytoplankton</b>			
$\alpha_1$	Half-saturation uptake diatoms	0.55	mmol-N m <sup>-3</sup>
$\alpha_2$	Half-saturation uptake flagellates	0.45	mmol-N m <sup>-3</sup>
$RD_0$	Maximum uptake diatoms at 0°C	1.50	d <sup>-1</sup>
$RF_0$	Maximum uptake flagellates at 0°C	0.75	d <sup>-1</sup>
$S_{DIA}$	Sinking rate diatoms	-1	m d <sup>-1</sup>
$Iopt_{dia}$	Optimum PAR diatoms	95	W m <sup>-2</sup>
$Iopt_{flag}$	Optimum PAR flagellates	105	W m <sup>-2</sup>
$k_c$	Attenuation constant self-shading	0.03	m <sup>2</sup> (mg Chl a) <sup>-1</sup>
$LPN$	Loss rate phytoplankton to nutrients at 0°C	0.03	d <sup>-1</sup>
$LPD$	Loss rate phytoplankton to detritus at 0°C	0.02	d <sup>-1</sup>
$Th_{S1}$	Half-saturation temperature diatoms	12	°C
$Th_{S2}$	Half-saturation temperature flagellates	7	°C
$Q_{10}$	Maintenance temperature coefficient	0.07	°C <sup>-1</sup>
$RFR$	Redfield ratio N:P (mol-based)	16:1	fraction
N:Si	Si:N-ratio (mol-based)	1.1	fraction
<b>Zooplankton</b>			
$Imax_{MEZ}$	Maximum grazing mesozooplankton at 12°C	0.47	d <sup>-1</sup>
$Imax_{MIZ}$	Maximum grazing microzooplankton at 0°C	0.60	d <sup>-1</sup>
$K_{MEZ}$	Half-saturation ingestion mesozooplankton	0.32	mmol-N m <sup>-3</sup>
$K_{MIZ}$	Half-saturation ingestion microzooplankton	0.60	mmol-N m <sup>-3</sup>
$AE_{MEZ}$	Assimilation efficiency mesozooplankton	0.65	fraction
$AE_{MIZ}$	Assimilation efficiency microzooplankton	0.60	fraction
$R_{MEZ}$	Active respiration mesozooplankton	0.29	fraction
$R_{MIZ}$	Active respiration microzooplankton	0.35	fraction
$\beta_{MEZ}$	Basal respiration mesozooplankton at 0°C	0.005	d <sup>-1</sup>
$\beta_{MIZ}$	Basal respiration microzooplankton at 0°C	0.03	d <sup>-1</sup>
$pref_{DI}$	Grazing preference for diatoms by MEZ and MIZ	1.0	fraction
$pref_{FL}$	Grazing preference for flagellates by MEZ and MIZ	1.0	fraction
$pref_{MIZ}$	Grazing preference for microzooplankton by MEZ	1.0	fraction
$Mmax_{MEZ}$	Maximum mortality mesozooplankton at 0°C	0.004	d <sup>-1</sup>
$Mmax_{MIZ}$	Maximum mortality microzooplankton at 0°C	0.030	d <sup>-1</sup>
$KM_{MEZ}$	Half-saturation mortality mesozooplankton	0.07	mmol-N m <sup>-3</sup>
$KM_{MIZ}$	Half-saturation mortality microzooplankton	0.02	mmol-N m <sup>-3</sup>
$Th_{SMIZ}$	Half-saturation temperature microzooplankton	4	°C
$SVM_{MEZ}$	Seasonal vertical migration mesozooplankton	0-25	m d <sup>-1</sup>
<b>Detritus and nutrients</b>			
$DN$	Mineralisation of detritus at 0°C	0.001	d <sup>-1</sup>
$DN_{Si}$	Mineralisation of Si-detritus at 0°C	0.0001	d <sup>-1</sup>



$NI_0$	Maximum nitrification rate at 0 °C	0.02	$d^{-1}$
$K_{nit}$	Oxygen half-saturation in nitrification	3.75	$mmol-O_2 m^{-3}$
$K_{denit}$	Nitrate half-saturation in denitrification	0.135	$mmol-NO_3 m^{-3}$
$T_{sen}$	Temperature coefficient on recycling processes	0.07	$^{\circ}C^{-1}$
$SEDR$	Sinking rate detritus	-20	$m d^{-1}$
RQN	Respiratory quotient in nitrification	2.0	$O_2:NO_3$
RQC	Respiratory quotient in detritus	1.0	$O_2:Organic-N$
$S_{DET}$	Settling rate detritus	20	$m d^{-1}$

897  
898



899

## 900 **10.2 Appendix B, the ocean model (HYCOM)**

901 The ocean model (HYCOM) has 40 hybrid vertical levels, combining isopycnals with z-level  
902 coordinates and sigma coordinates. Tides are included internally within the ocean model using  
903 eight constituents and similar tides are added at the open boundaries using the Oregon State  
904 University TOPEX/Poseidon Global Inverse Solution (TPXO 8.2,) Egbert and Erofeeva, 2002).  
905 More than 100 rivers are included as monthly climatological discharges obtained from the  
906 Global Runoff Data Centre (GRDC, <http://grdc.bafg.de>) and scaled as prescribed by Dai and  
907 Trenberth (2002)(Dai and Trenberth, 2002). In addition the globally gridded Core v2 runoff data  
908 (Large and Yeager, 2009) is added for Greenland, the Canadian Archipelago, Svalbard, and  
909 islands within the Arctic Ocean.

910 The sea-ice model (CICE) describes the dynamics and thermodynamics of the sea-ice as  
911 described by Rasmussen et al, 2018 (Rasmussen et al., 2018). The dynamics is driven by drag  
912 from wind and ocean, surface tilt of the ocean, Coriolis force, and the internal strength of sea ice  
913 that will resist movement of the ice pack. The internal strength is based on the Elastic-Viscous-  
914 Plastic (EVP) sea-ice rheology (Hunke, 2001), that originates from the Viscous-Plastic (VP)  
915 described by Hibler (1979)(Hibler, 1979). CICE includes 5 thickness categories of sea ice within  
916 each grid cell in order to describe the inhomogeneity. The thermodynamics prescribes a vertical  
917 temperature profile with a resolution of four sea ice layers and one layer of snow for each sea-ice  
918 category (Bitz and Lipscomb, 1999). Snow is very important for the thermodynamics of sea ice  
919 as it insulates sea ice from the atmosphere and has a higher albedo than sea ice. The lower  
920 boundary is governed by the upper ocean temperature, which is usually the ocean freezing  
921 temperature and is linearly dependent on its salinity. The upper boundary is governed by the heat  
922 and radiation transfer between the atmosphere and the combined snow/ice surface. The net heat  
923 flux is calculated based on the 2m atmospheric temperature, humidity, incoming long and short-  
924 wave radiation, and 10m wind and the state of the surface of the sea-ice model.

925 The HYCOM and CICE models used in this paper are coupled on each time step using the Earth  
926 System modeling Framework (ESMF) coupler (Collins et al., 2004). The HYCOM-CICE set-up  
927 at DMI used in this paper covers the Arctic Ocean and the Atlantic Ocean, north of about 20°S,  
928 with a horizontal resolution of about 10 km (Madsen et al., 2016)..





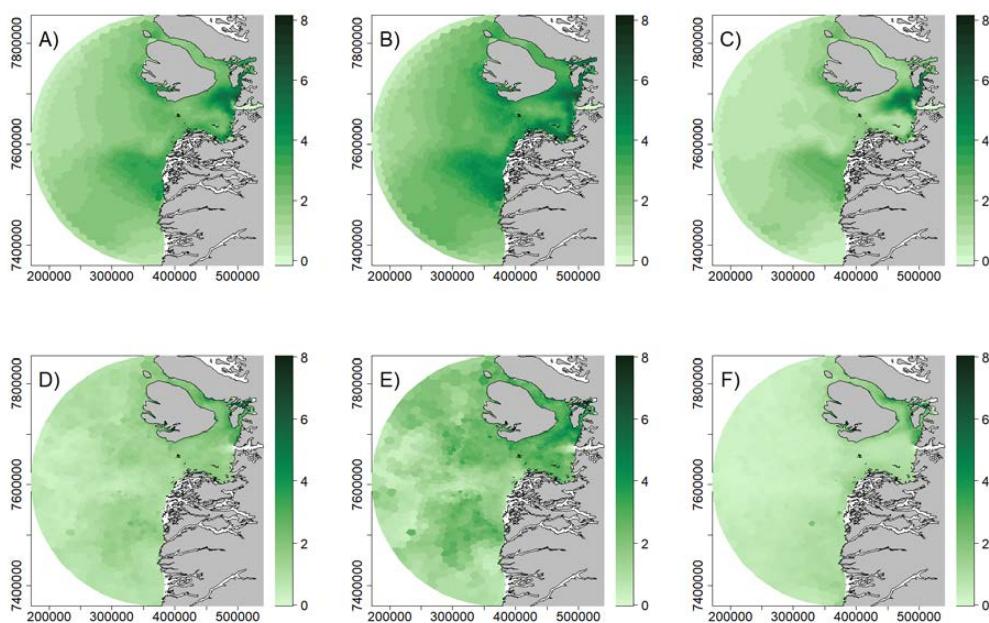
929 The HYCOM-CICE model system assimilates re-analyzed sea-surface temperature  
930 (<https://podaac.jpl.nasa.gov/GHRSST>, Høyer et al., 2012, 2014) and sea-ice concentration  
931 provided by the EUMETSAT Ocean and Sea Ice Satellite Application Facility (OSI SAF,  
932 [www.osi-saf.org](http://www.osi-saf.org), Lavergne et al., 2019) on a daily basis. The model is initialized in summer  
933 1997 using the Polar Science Center Hydrographic Climatology (PHC; Steele et al., 2001) in the  
934 Arctic Ocean and World Ocean Atlas 2001 0.25° (Conkright et al., 2002) in the Atlantic, with a  
935 100 km linear transition. The atmospheric forcing is obtained from the Era-Interim reanalysis  
936 (Dee et al., 2011) until 2017 and thereafter deterministic HRES ECMWF forcing  
937 ([www.ecmwf.int](http://www.ecmwf.int)).



938 **10.3 Appendix C, Figures**

939

Figure C1: Surface Chl *a* concentration (mg chl *a* m<sup>-3</sup>) in 2010 obtained from the model (A-C) and from remote sensing (D-F). A) and D) are annual averages, B) and E) are April-June averages, and C) and F) are July-September averages.

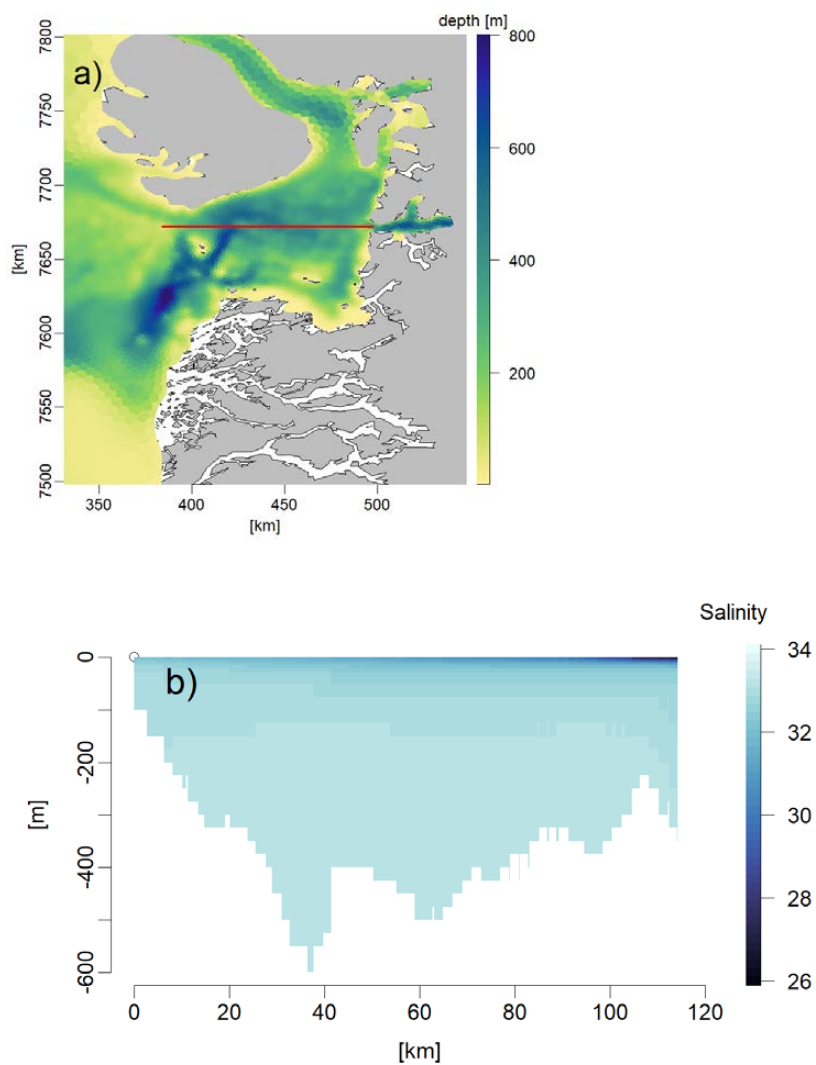


940



941

Figure C2: a) Position and b) bathymetry of transect (x-axis: distance in km, y-axis: depth in m) shown in Figure C3.



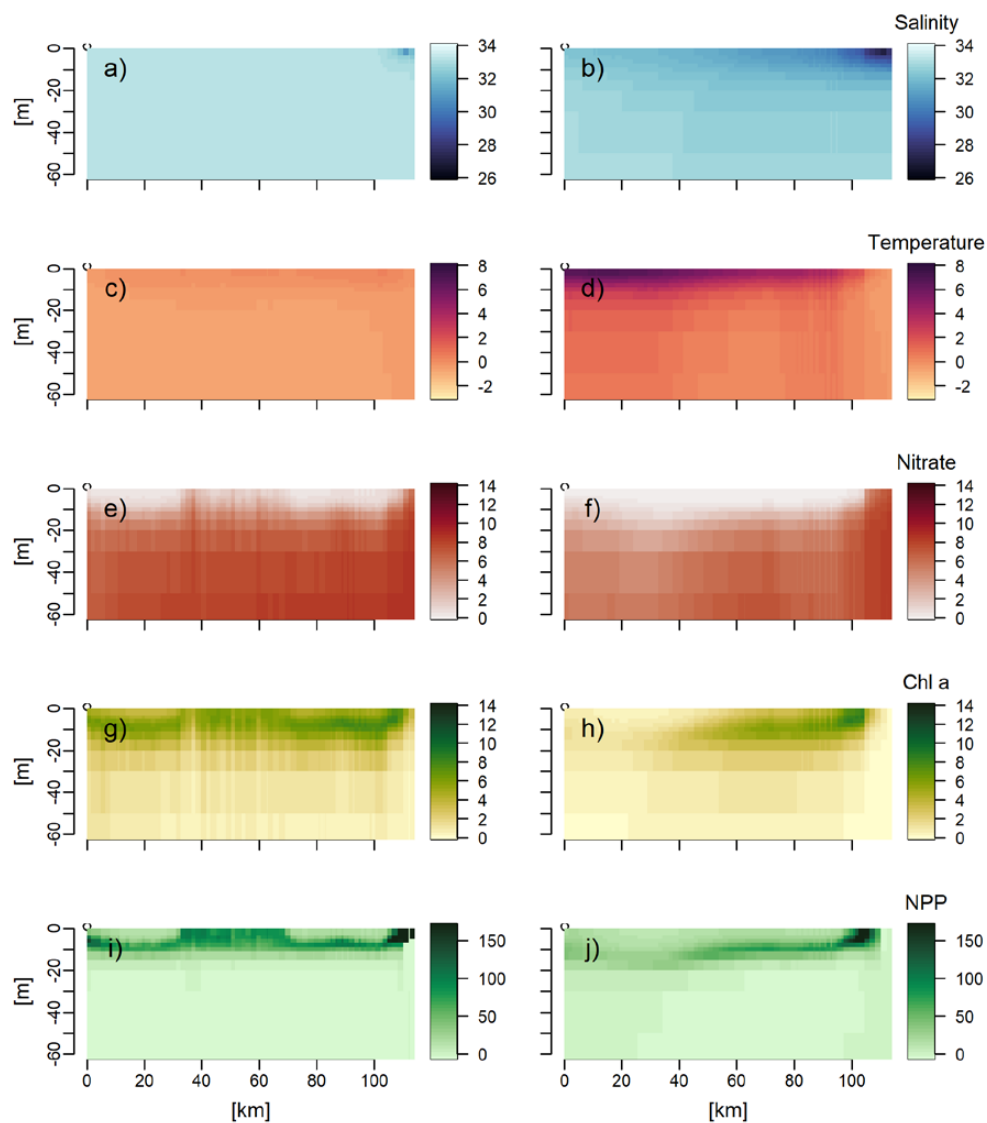
942

943



944

Figure C3: Transects (x-axis: distance in km, y-axis: depth in m) of salinity (a, b) temperature (°C) (c, d), DIN ( $\text{mmol m}^{-3}$ ) (e, f), Chl *a* ( $\text{mg m}^{-3}$ ) (g, h) and NPP ( $\text{mgC m}^{-3} \text{d}^{-1}$ ) (i, j) in April (left) and August (right) 2010 along the transect shown in figure C2:



945